NTNU
Norwegian University of
Science and Technology

Comparative numerical and experimental study of the global responses of the spar-torus-combination in extreme waves due to the bottom slamming effect

Massimiliano Saletti

NORWEGIAN UNIVERSITY OF SCIENCE AND TECHNOLOGY

AND

TECHNICAL UNIVERSITY OF DENMARK

Comparative numerical and experimental study of the global responses of the spar-torus-combination in extreme waves due to the bottom slamming effect

---

Author:
Massimiliano Saletti

Supervisors:
Prof. Zhen Gao (NTNU)
Prof. Harry B. Bingham (DTU)
Co-Supervisor:
Postdoc Jiang Zhiyu (NTNU)

TRONDHEIM 2018

Summary

The purpose of this graduation thesis *Comparative numerical and experimental study of the global responses of the spar-torus-combination in extreme waves due to the bottom slamming effect* is to investigate the effects of nonlinear loads caused by slamming on the spar torus combination (STC) concept.

The STC concept is a device that integrate wind and wave energy and is composed of a 5 MW spar-type floating wind turbine and an axisymmetric wave energy converter (torus) that heaves along the spar to extract energy from waves through a hydraulic power take-off system (PTO). Among renewable energy resources, both offshore wind and wave energy have a great potential. However, the development of wind energy technology has already been commercialized while wave energy technology is still immature. In order to bring offshore renewable energy applications closer to the market, structures like the STC have been proposed under the European Commission FP7 Marine Renewable Integrated Application Platform [1] (MARINA PLATFORM) project. Several benefits might be identified from the integration of wind and wave energy devices in one single structure, such as the reduced investment cost derived from the use of the same infrastructure, the positive synergy in terms of dynamic responses of the structure and augmentation of the produced power [2].

Experimental data for this thesis were collected at Sintef Ocean for different survival modes proposed for the STC to ensure the structural integrity under extreme environmental conditions due to large wave forces on the torus. Tests performed in the Mean Water Level (MWL) survival mode, where the torus is fixed to the spar at mean water level, highlighted water exit and entry phenomena due to excessive heave motions of the floater, which leads to significant wave slamming loads on the bottom of the torus.
Nonlinear hydrodynamic properties have been studied in order to compare the experimental results with the time-domain code SIMO [3], which is based on the linear potential theory. A simplified nonlinear wave load model in SIMO (which is basically a correction of the linear model considering the nonlinear buoyancy force, the nonlinear Froude-Krylov force, and the slamming force) have been developed and implemented, with focus on the interface forces between the torus and the spar.
Slamming phenomena have been investigated applying the strip-theory approach in the local x-direction. For each strip, the local Wagner-type solution is considered. Moreover, nonlinear Buoyancy and Froude-Krylov force have been studied using both pressure integration and Sclavounos [40] methods and implemented in SIMO.

On the basis of the results of this research, it can be concluded that it is possible to reach good agreement between experimental and numerical results implementing in SIMO the nonlinear loads.

The author recommends further modification on the model in SIMO in order to be able to implement Wagner's slamming solution. Furthermore a structural assessment on the structure should be carried out considering the slamming force and the vibrations that it generates.

Preface

This thesis is an original work by Massimiliano Saletti. No part of this thesis has been previously published.

I would like to give my sincere thanks to my supervisors, Professor Zhen Gao at Norwegian University of Technology and Science (NTNU) and Professor Harry B. Bingham at Technical University of Denmark (DTU), for providing me significant guidance and help on my research. Their careful and effective supervision during this study significantly helped me in solving many problems.

Dr. Zhiyu Jiang, as my co-supervisor, contributed great time and efforts to the discussion and guidance on my research. I really appreciate his contributions and efforts.
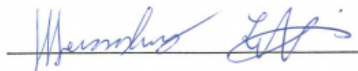
I also appreciate the help from Dr Ling Wan who provided me the results of the experiments collected at Sintef Ocean and for the work he have done in his Phd Thesis which has been the starting point for my Thesis.

Finally, I would like to thank my family, for their encouragement, support and love.

Trondheim, Norway   Massimiliano Saletti

June 11, 2018

Table of Contents

List of Tables

List of Figures

Abbreviations

DLL	=	Dynamic Link Library
D.O.F.	=	Degree of Freedom
FWEC	=	Floating Wave Energy Converter
FWT	=	Floating Wind Turbine
HAWT	=	Horizontal Axis Wind Turbine
LSD	=	Limit State Design
MARINA	=	Marine Renewable Integrated Application
MRE	=	Marine Renewable Energy
MWL	=	Mean Water Level survival mode
OWC	=	Oscillating Water Column
PTO	=	Power Take Off
SFC	=	Semi-submersible Flap Combination
STC	=	Spar Torus Combination
SWL	=	Still Water Line
TLP	=	Tension Leg Platform
VLFS	=	Very Large Floating Structure
WEC	=	Wave Energy Converter
WEE	=	Water Entry and Exit
WOD	=	Water On Deck
WT	=	Wind Turbine

Introduction

1.1 Background

According to most climate scientists, human activities, after the pre-industrial period, created an extreme change in Earth climate [4]. Global warming trend caused by the expansion of the "greenhouse effect" has been proved to be almost ten times faster than the average rate of ice-age-recovery warming [5]. Studies shows that among the gasses that increase the greenhouse effect, a main role is played by the carbon dioxide, which level in the atmosphere rapidly increased after the Industrial Revolution and is still growing as it can be clearly seen from Figure 1.1.

Effects that result from global climate change and that are visible nowadays are: loss of sea ice, shrunk of the glaciers, changes in precipitation patterns, stronger and more intense hurricanes, increasing of the sea level, more droughts and heat waves,etc. [6]. Moreover, if species will not adapt to new climate patterns, the global worming will lead to a loss of species [7].
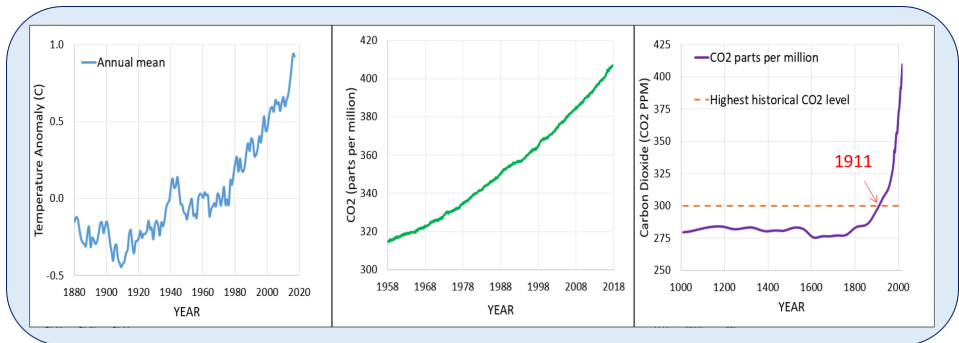
Figure 1.1: Change in global surface temperature, CO_2 levels measured at Mauna Loa Observatory, Hawaii, in recent years, comparison of atmospheric samples contained in ice cores and more recent direct measurements of the atmospheric CO_2[6] in order from the left.

Looking at the major sources of anthropogenic CO_2 emissions in Figure 1.2 is clear the main role played by the production of electricity.
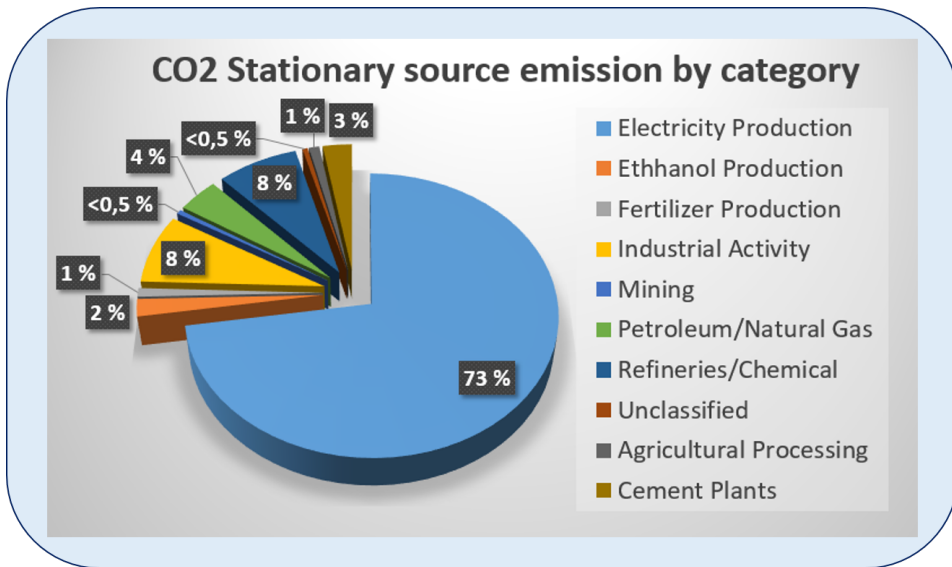
Figure 1.2: Major sources of anthropogenic CO_2 emissions [8].

Emissions can be lowered by becoming energy efficient and by progressing towards an energy system based on fuels with low, or no-carbon, content (de-carbonisation). Environmental friendly policy have been applied in many countries and are rising the production of renewable energy tanks to new installation but also to the large investment in research that allows to produce more efficient devices.

Marine Renewable Energy (MRE) represents a treasure trove of powerful winds, waves and tides whose energy could be harnessed to relieve dependence on conventional forms of energy. The EU is actively developing programmes to support this renewable alternatives [1].

1.2 Wind energy and offshore wind turbine

Wind power has been harnessed by humans since early recorded history. In the past, wind-powered machines have been used to ground grain and to pump water. The first windmill used for the production of electric power was built in Scotland in July 1887 by Prof James Blyth of Anderson's College, Glasgow [9]. A significant impulse to the use of wind as energy resource has been given from the oil crisis of 1973 [10].

A wind turbine is a machine that transforms kinetic energy in the wind to mechanical energy using a shaft and then into electrical energy in a generator. A typical modern wind turbine presents the following characteristics [11]:

- Horizontal axis wind turbine (HAWT);

- Upwind;

- Three-bladed;

- Pitch-regulated;

- Variable speed.
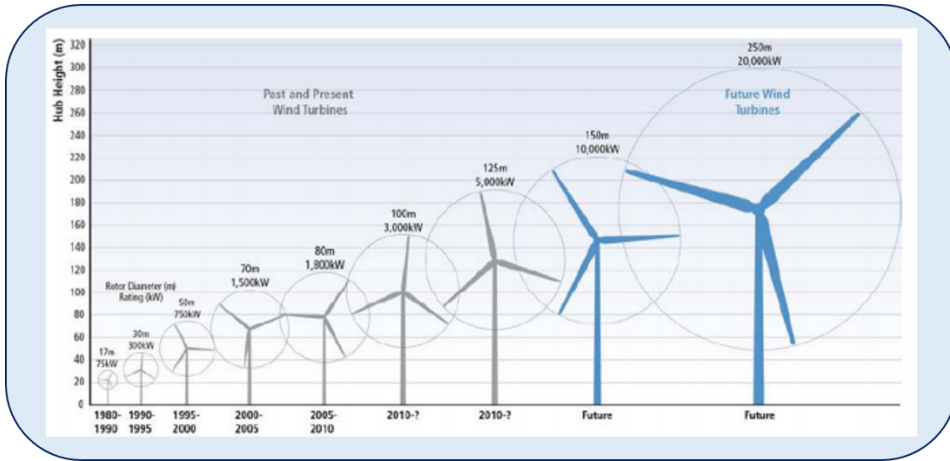
Figure 1.3: Development of wind turbines in size [11].

From the study of the basic aerodynamics for wind turbines it is possible to define a power coefficient, C_P as the ratio between the actual power obtained by a wind turbine and the maximum available power in wind. Furthermore a theoretical upper limit of the aerodynamic efficiency for wind power extraction is denoted by the Betz limit, and is 0.593.

The gradual upscale of machines (shown in Figure 1.3) and the developments on both the structure and the rotor, allowed to reach an efficiency of 0.5 (2000s) [11] and to reduce the maintenance costs.

The increasing interest in the use of wind energy can be clearly seen from Figure 1.4 where the global power capacity and annual additions are plotted.

The installation of wind turbines is not limited to the land-based WTs but also to turbine installed offshore. Offshore wind farms presents several advantages such as the absence of noise and visual impact moreover they work in favorable conditions (higher wind velocity and less turbulent wind) and the transportation is somehow easier than on land. On the other hand the offshore WTs presents some cons: the working environment is more corrosive, the loads on the structures are higher, the access for installation and maintenance is more complicated.

Figure 1.5 shows the increasing power offshore global capacity. The main issue of offshore WT is represented by the depth limitation of the classic bottom-fixed turbines. Many countries does not have wide areas with shallow water (<45m) as for example USA, Norway and Japan.
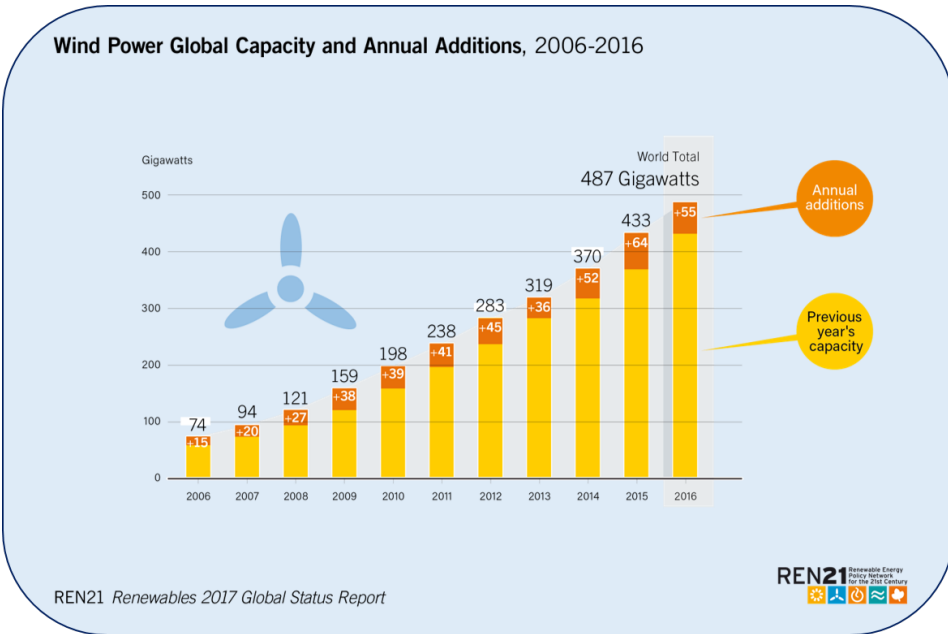
Figure 1.4: Global power capacity and annual additions, 2006-2016 [12].
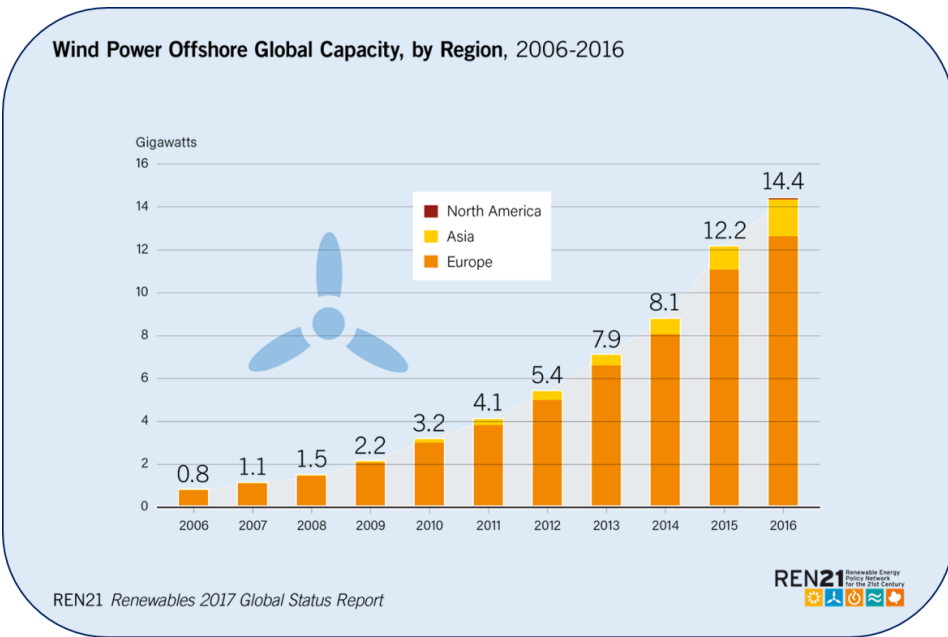
Figure 1.5: Wind power offshore global capacity, by region, 2006-2016 [12].

For all the sites with water depths greater than 50 m, the floating wind turbine (FWT) concepts are more feasible and competitive. Floating foundations for WT, as it can be observed from Figure 1.6, can generally be categorized into three main types [13]:

- Spar

- Tension leg platform (TLP)

- Semi-submersible
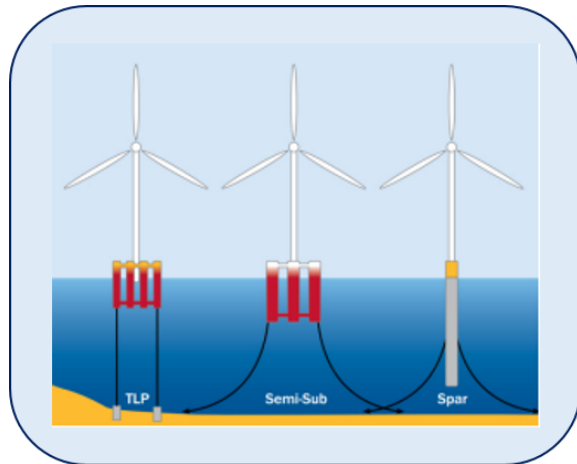
Figure 1.6: Floating offshore wind turbine substructures [2].

The choice of one system over the others depends on the water depth, the environmental conditions, the installation and from the distance to shore.

The three different floating foundations mentioned above are characterized from different physical principle or strategy that are used to achieve static stability [15]:

1. Ballast: used in Spar-buoys platforms. Stability is achieved by using ballast weights hung below a central buoyancy tank which creates a righting moment and high inertial resistance to pitch and roll and usually enough draft to offset heave motion.

2. Mooring Lines: used in TLP platforms. Stability is achieved through the use for mooring line tension.

3. Buoyancy: used in Semi-submersible platforms. Stability is achieved through the use distributed buoyancy, taking advantage of weighted water plane area for righting moment.

Even though the use of floating wind turbines is still limited, increasing interest on this type of foundations is shown in Figure 1.7 where the floating offshore wind market grows prevision is plotted.

The first world floating wind park has been installed in Scotland from Statoil [14] and started to produce electricity in October 2017.
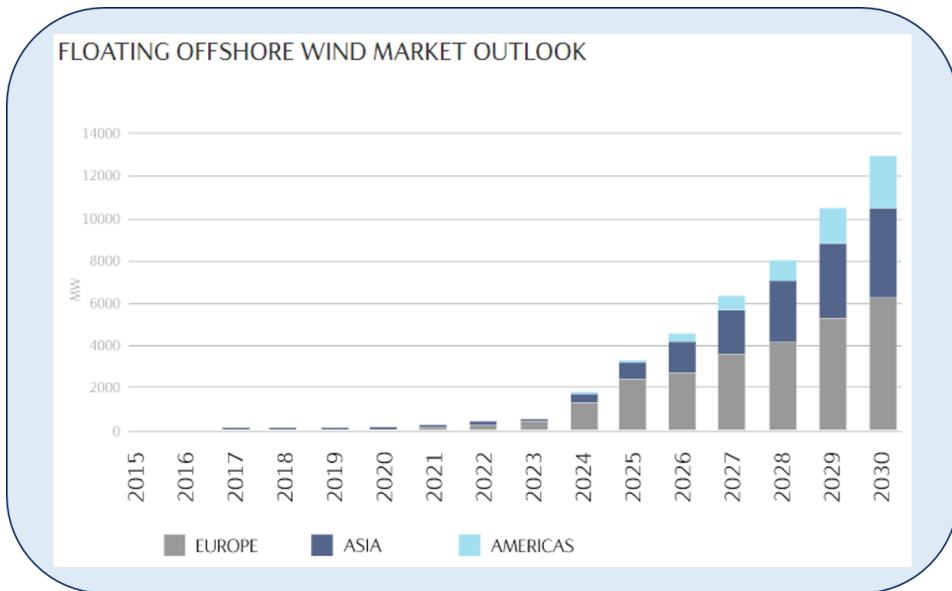
Figure 1.7: Floating offshore wind market outlook [14].

Being the Spar the type of floating foundation at the base of the structure studied in this Thesis some more information are provided in the following subsection.

1.2.1 Spar-type wind turbine

Main advantage of the spar-type foundation is the good performance in heave motion. The good behaviour in have motion comes from the deep draft and the small water plane area, characteristics that distinguish the spar WT, as it can be seen from Figure 1.15. This characteristics can reduce the first-order wave force and mean drift force. On the other hand the spar presents poor performance in pitch and roll motions [2].
The main disadvantage of the spar-type foundation is the requirement of large water depth, indeed it cannot be used in less than 100 m of water depth, due to the necessary draft. The large draft could make major maintenance difficult and expense [16].

Figure 1.8: Spar wind turbine [14].

1.3 Wave energy and wave energy converters

The idea of generating energy from ocean waves interested man for centuries. The first known device was patented in Paris by two Frenchmen in 1799 and was a shoreline device made to pump fresh water to a nearby village. Since that initial idea development in the area has been sporadic. The interest in wave energy had two real boom periods, one in the 1970s and one that which began in the mid-1990s. As for the wind energy, the driver of the 1970s boom was the oil crisis [17].

Being the total wave energy resource of the same order of magnitude as world electricity consumption (∼2 TW) this energy source could give a significant contributor to human energy demands, even not representing a panacea [18]. The exploitable limit is probably at most about 10-25%, in the areas where the ocean-wave energy is more persistent and spatially concentrated [19].

What slow down the development of the wave energy converter (WEC) is the theoretical difficulty of the hydrodynamic process that governs the wave energy absorption together with the difficulty related to the conception of the power take-off mechanism (PTO).

The physical law that governs the operation of a WEC is the conservation of energy. The WEC interact with the waves in order to reduce their amount of energy that is otherwise present in the sea [19]. Wave energy has high energy density and is proportional to the wave period and to the square of wave amplitude [2].

Several way to classify wave energy systems can be considered, but if the principle of absorbing wave energy is analyzed, the following categorization can be done [20]:

- oscillating bodies

- oscillating water columns

- overtopping devices

as shown in Figure 1.9.
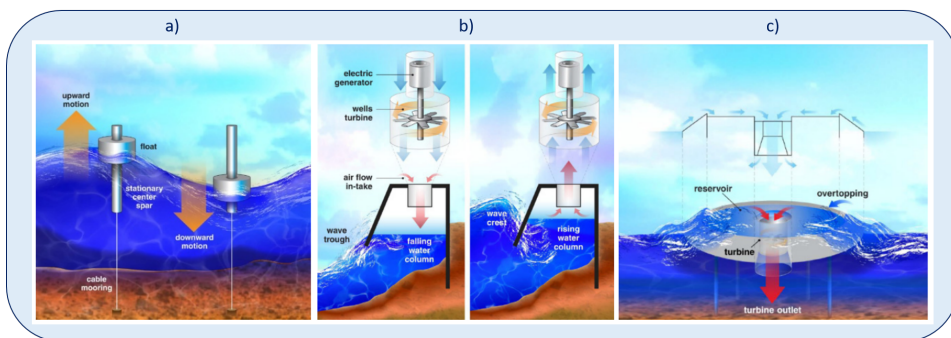
Figure 1.9: Basic principles of absorbing wave energy: a) oscillating bodies, b)oscillating water columns, c) overtopping devices [2].

Being the Wavebob concept the type of oscillating body at the base of the structure studied in this Thesis some more information are provided in the following subsection.

1.3.1   Wavebob concept and other oscillating bodies technology

Oscillating bodies extract wave energy by the oscillation of the structure relative to a floating or fixed structure using a PTO system that can convert the wave power into mechanical or electrical energy. PTO system can be classified as [18]:

Figure 1.10: Wavebob concept [22].

- air turbine

- linear generators

- hydraulic system

Oscillating bodies can be both floating or fully submerged.
The disadvantages of the oscillating bodies are the mooring system, the access for maintenance and the need of long underwater electrical cables.
Another possible categorization of oscillating bodies can be considered as follows [20]:

- Single-body heaving buoys. The simplest oscillating-body device is the heaving buoy that react against a fixed frame of reference that can be either the sea bottom or a bottom-fixed structure. Such systems are usually conceived as point absorbers which means that their horizontal dimensions are much smaller than the wavelength. An alternative design consists in a buoy that is connected to a bottom-fixed structure by a cable which is kept tight by a spring or similar device. The relative motion between the wave-activated float on the sea surface and the seabed structure activates a PTO system.

- Multi-body system in which the energy is converted from the relative motion between two bodies oscillating differently. This configuration avoid the difficulties of single floating body related to the distance between the free surface and the bottom and/or to tidal oscillations in sea level but introduces special control problems.

- Fully submerged heaving systems that as the other two system mentioned are nominally heaving systems, i.e. the energy conversion is associated with a relative translational motion.

- Pitching devices in which the energy conversion is based on relative rotation (mostly pitch) rather than translation.

- Bottom-hinged systems in which a single oscillating-body device operate in pitching mode and are based on the inverted pendulum hinged at the sea bed concept.

- Many-body systems where the device consists of a large set of floating point absorbers that react against a common frame and shares a common PTO.

The Wavebob, which has been developed in Ireland between 1999 and 2013 [24], is a two-body heaving device [23] that use the circular wave motion to move the PTO in the vertical direction capturing the energy of the wave [22]. A schematic representation of this device is presented in Figure 1.10. The structure consists of two co-axial axisymmetric buoys, whose relative axial motions are converted into electric energy through a high-pressure-oil system. The inner buoy is rigidly connected to coaxial submerged body located underneath, whose function is to increase the inertia and allow the tuning to the average wave frequency.

1.4 Combined wind and wave energy converters

Multi-purpose platforms for marine renewable energy (MRE) are a great promise for the future in order to exploit as much power as possible in an offshore field. The combination of different energy devices in the same structure could bring considerable environmental and economic benefits [25]. Different combination are possible, for example combining offshore wind farms, marine aquaculture or the wave and tidal energy converters [2].
To stick to the argument of this project only the combination of wind and wave are going to be considered.
Offshore wind and wave energy are always related which means that in the same field it is possible to use the same structure to exploit both wind and wave power reducing the investment, creating a positive synergy in terms of dynamic responses of the structure and augmenting the produced power. Unfortunately, the combination of two different system that are still not completely known is anything but trivial.
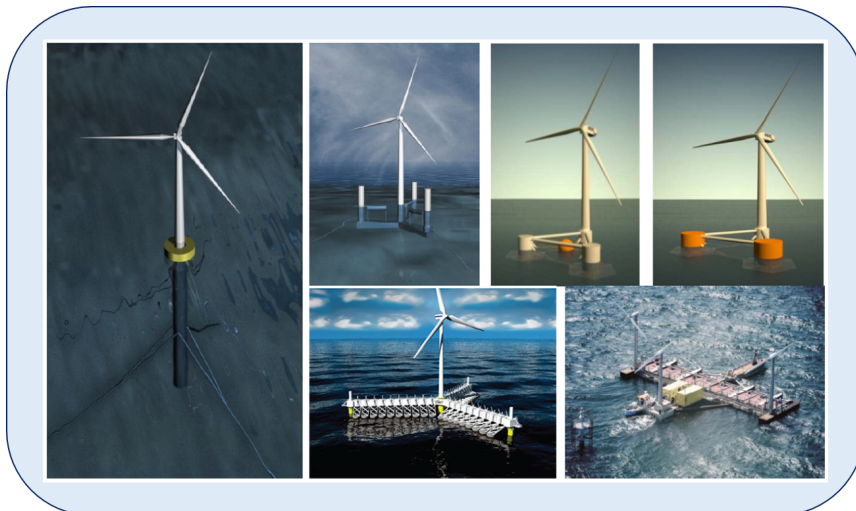
Figure 1.11: Some of the wind and wave energy devices studied. From top left: STC concept, SFC, WindFloat+OWC, WindFloat+point absorber, Wavestar+wind turbine, and Floating Power Plant [2].

Some of the challenges that can be identified in the combined concepts are [2]:

- survivability in extreme sea states

- limited experience with model tests

- numerical analysis require tools with strongly nonlinear features

- design of the interface between FTWs and WECs that ensure functionality

- power output optimization in order to achieve higher effcency

The European Commission FP7 Marine Renewable Integrated Application [1] Platform project is a project in which the integration of wind and wave energy devices on a single platform have been studied focusing on floating concepts for deep water applications. Among the project studied there are the spar-torus combination (STC) concept, the semi-submersible flap concept (SFC) and the oscillating water column (OWC) array with a wind turbine, as shown in Figure 1.11.

1.4.1 The Spar-Torus Combination concept

Concept

The STC concept, shown in Figure 1.12, consists of a spar floater to support a 5 MW wind turbine and an axisymmetric wave energy converter (torus) that heaves along the spar to extract energy from waves through a hydraulic PTO system. It is moored by a three-line catenary system. The reference wind turbine selected is the NREL 5 MW [26] while the WEC model is the Wavebob.
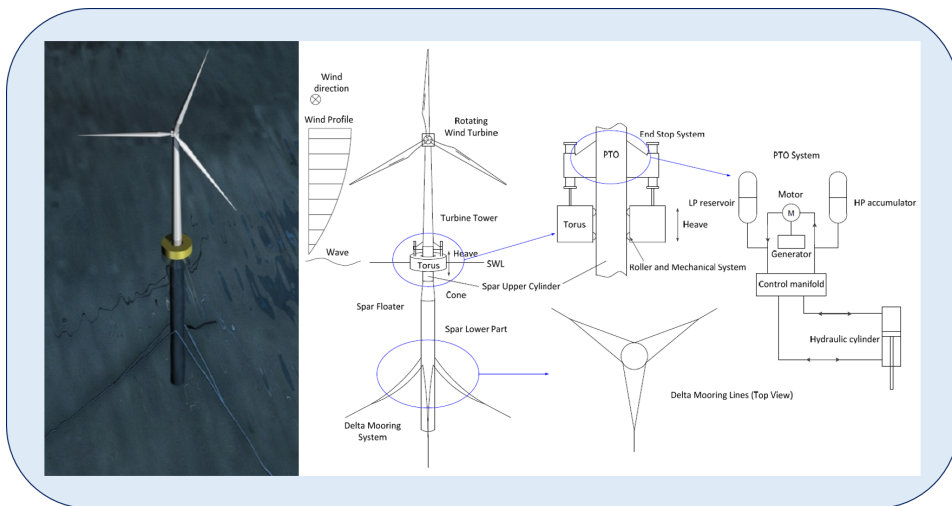
Figure 1.12: STC concept and components [2].

- NREL 5 MW:
  The reference 5 MW Horizontal-Axis Wind Turbine converts the wind power. As shown in Figure 1.13 the cut in is at 3 m/s, the rated at 11.4 m/s and the cut out at 25 m/s. The configuration of the control system adopted for the three blade wind turbine is a conventional variable speed, variable blade-pitch-to-feather. In order to maintain constant the generator power when the wind speed increase (flat part of the second graph in Figure 1.13) the blade-pitch control is activated. In extreme wind conditions, the wind turbine is shut down and parked and the blade are aligned to the wind to reduce the aerodynamic loads.
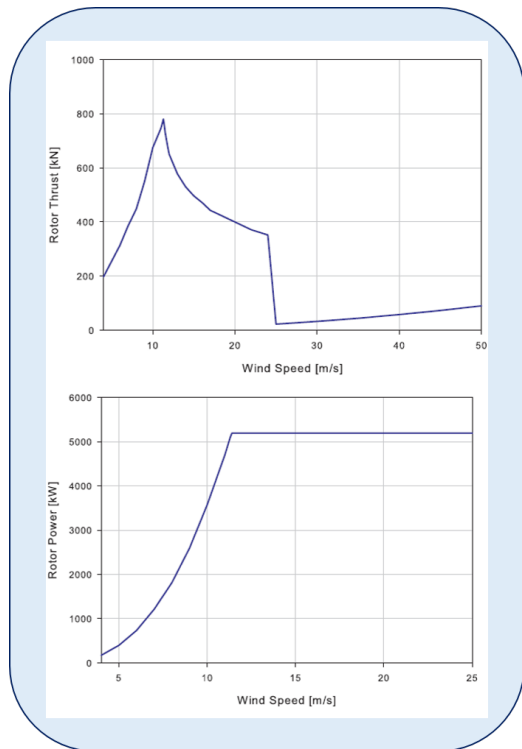
Figure 1.13: Rotor thrust and power curves at different wind speeds at full scale [26].

- Wave energy converter:
  The torus is free to move in the vertical direction along the spar without large frictions thanks to the rollers and to a mechanical system. The relative heave motions of the torus respect to the spar is absorbed by an hydraulic PTO system. The hydraulic circuit of the power take off stores the energy in an high pressure (HP) accumulator. As it can be seen from the schematic sketch in Figure 1.12, the PTO is also equipped with a low pressure (LP) reservoir, which aim is to smooth the absorbed irregular power. The energy is then converted by an hydraulic motor that produce electricity trough an electrical generator. The WEC has a rated power of 0.5 MW [2]. Moreover a system is installed in order to limit the heave motion in operational conditions. A mechanical brake is present to stop the relative motion of the torus in extreme conditions or in case of emergency.

- Mooring system:
  the offshore site for which the STC concept have been designed is located 30 km from the west coast of Norway [27]. For the installation in this area a delta-shaped mooring system is used in order to provide an additional yaw stiffness and damping to prevent excessive yaw motion [2].

Basic parameters of the STC

In Table 1.1 are presented the dimensions of the different parts that compose STC.
The spar-type FWT is composed by:

- wind turbine

- tower

- mooring system

- spar lower part

- spar upper part including the cone structure.

The wave energy converter is installed on the upper part of the spar.

Spar floater	Design values
Total length	130 m
Draft	120 m
Lower part diameter	10 m
Lower part length (including cone)	110 m
Upper part diameter	6.5 m
Upper part length	20 m
Fairlead position for mooring	-70 m (From SWL)
Tower	**Design values**
Diameter	6.5 m
Length	77 m
Tower base position	10 m (From SWL)

Wind Turbine	Design values
Rated power	5 MW
Rotor diameter	126.3 m
Nacelle mass	110 m
WEC	**Design values**
Rated power	0.5 MW
Height	8 m
Inner diameter	8 m
Outer diameter	20 m
Draft	4 m

Table 1.1: Design dimensions of the different parts of the STC [2].

The natural periods and damping ratios of the STC have been identified from the decay test performed in the model test. The results are presented in Table 1.2.

D.O.F.	Surge	Sway	Spar heave	Torus heave	Roll	Pitch
Natural periods [s]	81.3	84.4	30	6.4	40.1	39.5
Damping ratios [%]	5	7	-	-	3	3

Table 1.2: Results from the decay test [2].

From the table above it is possible to notice that the natural periods in surge, sway, roll and pitch are the same for the spar and for the torus while the motion in heave is different.

Survival modes proposed for the STC

When the wind speed reaches 25 m/s the wind turbine should be parked, while the torus should be in the non-operational mode when significant wave height is larger than 6 m. Four different survival modes have been proposed for the spar torus combination concept.

The main purpose of this survival modes is to reduce the wave loading on the WEC or to transfer the wave energy on the WEC to other types of energy [2]. Common features of all the survival modes are:

- turbine parked

- PTO system is released.
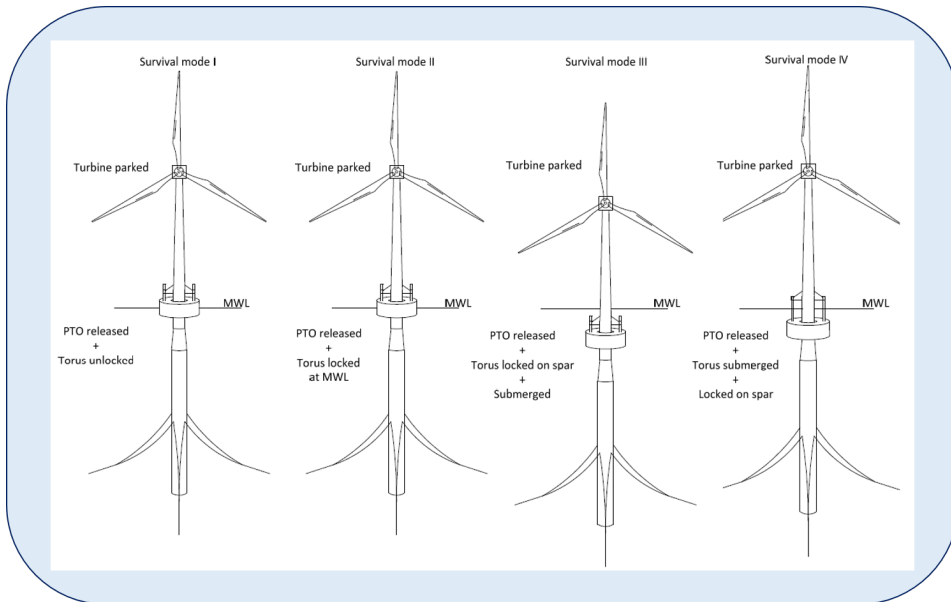
Figure 1.14: STC different survival mode proposed [2].

As shown in Figure 1.14, the characteristics of the four survival modes are:

- Mode I or released survival mode: the torus is free to move along the spar and its motion is limited only by the end stop system.

- Mode II or MWL: the torus is locked mechanically to the spar at the mean water level (MWL).

- Mode III or SUB: as for Mode II the torus is locked mechanically to the spar, but in this case ballast is added to the torus or to the bottom of the spar and the two bodies are submerged to a specifically position.

- Mode IV: the torus is ballasted by sea water and submerged until the end stop limit position.

Mean water level survival mode

In extreme wave conditions when STC is in the MWL configuration mode, water exit and entry phenomena have been observed due to excessive heave motions of the floater, which leads to significant wave slamming loads on the bottom of the torus. The cases in which this phenomena were observed are listed in Table 1.3.

	T [s]	9	11	12	13	14	15	17	19	21	23
H	2 m			▓	▓						
H	9 m	█	█	█	█	█	█				

Table 1.3: Occurrence of the nonlinear phenomena in the MWL survival mode. Strong WEE in case of wave height of 9 m and WEE in the case of wave height of 2 m [2].

Furthermore, Table 1.4 shows the natural periods and the damping ratios at full scale for the MWL survival mode founded from the decay tests done at MARINTEK.

D.O.F.	Surge	Sway	Heave	Roll	Pitch
Natural periods [s]	98	93.1	12.8	36	36.6
Damping ratios [%]	4.4	-	6.5	-	4

Table 1.4: Natural periods and damping ratios for the MWL survival mode [2].

Due to the resonant behaviors and the strongly nonlinear phenomena in the MWL survival mode the numerical analysis in the time-domain code SIMO [3], which is based on the linear potential theory, cannot provide reliable results. So, the numerical analysis require a nonlinear numerical model based on a nonlinear potential-flow solver [28, 29] considering a local impact solution for bottom slamming events and an approximate model for the water shipped on the deck.

Another way to numerically predict the behaviour of the STC in the MWL survival mode is to develop and implement a simplified nonlinear wave load model in SIMO. In order to account for the strongly nonlinear features, nonlinear buoyancy force, nonlinear Froude-Krylov force, and a simplified slamming force need to be incorporated.

Figure 1.15: Mean water level survival mode.

Furthermore in order to guarantee the structural integrity under extreme sea state for the MWL mode condition the limit state design (LSD) should be carried out considering the large local pressure on the torus due to slamming or wave forces.

1.5 Theoretical Background

1.5.1 Description of the problem

In order to predict the dynamic response of the STC a global integrated analysis is needed. If the STC is in operational conditions in order to evaluate the dynamic response it is necessary to investigate the rigid body motions, the relative motions between spar and torus, the mooring line forces, the PTO forces, the absorbed power, and further the strongly nonlinear effects such as water entry and exit, as well as the wave impact on the structure [2].

For the study of the interface vertical forces acting on the torus for the mean water level survival mode, object of this Thesis, some simplification on the integrated analysis can be applied. In the MWL survival mode the torus is locked to the spar which means that the torus is not heaving along the spar. This implies that there are no PTO force component, no friction force between the two structures and no force is generated for stopping the motion of the torus.

In the MWL survival mode strong nonlinear loads, that could compromise the integrity of the structure, act on the STC. It has been found that the phenomena like the water entry and exit (WEE) phases, water on deck (WOD) and slamming (SLA) appears for incident-wave with periods within the resonance region of heave motion. The structure has been tested for different wave height and periods. This work focus mainly on the analysis of the slamming loads which, for regular wave tests, appears for wave height of 9 m. Table 1.5 shows the different wave periods that have been considered.

Wave Height [m]	Wave Period [s]
9	11
9	13
9	15

Table 1.5: Analyzed regular wave tests with occurrence of strongly nonlinear phenomena.

In order to account the nonlinear phenomena in the numerical study of the motion of the structures in the linear time-domain SIMO it is necessary to add to the equation of motion, which is solved at each time step by the code, the nonlinear loads.

The study of the vertical forces acting on the torus requires an accurate analysis of the time series in order to determine the occurrence of the slamming phenomena. The slamming loads are really sensitive to the impact angle which need to be considered. This relative angle of the structure at the time of the impact is given by the difference between the pitch of the STC and and the local wave's steepness. Furthermore during this test the torus passes from being totally submerged to be out of water which means that nonlinear buoyancy and Froude-Krylov forces need to be taken into account.

To study this complex problem is essential to understand the hydrodynamic loads and the motions that these induces on the structure. To do that, the terms of the equation of motion have to be analyzed and a more detailed investigation on the slamming phenomena is necessary. Being the WT parked in the extreme operational conditions it has been decided to not analyze the aerodynamic loading, that are dominant in the operational conditions.

1.5.2 Hydrodynamic loading

The hydrodynamic forces on an offshore floating structures, considering the potential flow theory, can be divided into wave excitation forces and radiation forces as shown in Figure 1.17.
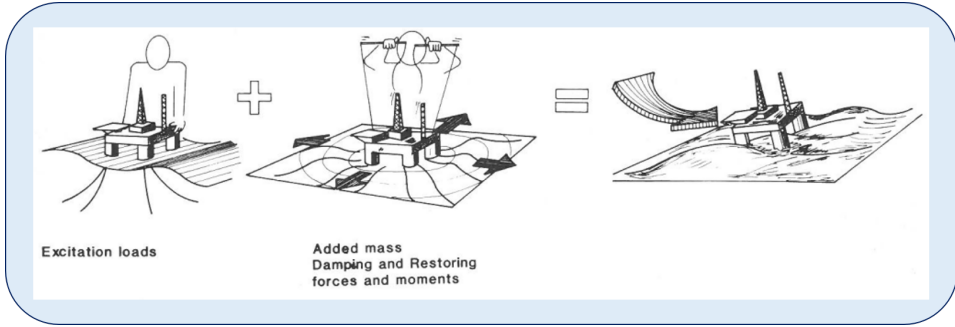
Figure 1.16: Decomposition of the linear wave-structure interaction problem [35].

From the first term of the equation sketched in Figure 1.17 it can be seen that the excitation forces are caused by the incoming regular waves when the structure is restrained from oscillating. The excitation forces include the Froude-Krylov force caused by the undisturbed wave pressure field and the diffraction force caused by the existence of the body in the waves. The second term of the equation shows how radiation forces are caused by the body motions with the wave excitation frequency. In this second case there are no incident waves and the hydrodynamic loads generated by the oscillation of the body are the added mass, damping and restoring.

Summing the incoming wave velocity potential (Φ_I) to the diffraction potential (Φ_D) and to the radiation potential (Φ_R) the total velocity potential can be defined as:

$$\Phi = \Phi_I + \Phi_D + \Phi_R \tag{1.1}$$

Moreover, the incident wave dynamic pressure and the diffraction dynamic pressure along the mean wetted surface and the radiation forces can be written as:

$$\mathbf{F_{ext}}(t) = -\int_{S_{0B}} \rho \frac{\partial \Phi_I}{\partial t} \mathbf{n} dS - \int_{S_{0B}} \rho \frac{\partial \Phi_D}{\partial t} \mathbf{n} dS \tag{1.2}$$

$$\mathbf{F_{rad}}(t) = -\int_{S_{0B}} \rho \frac{\partial \Phi_R}{\partial t} \mathbf{n} dS \tag{1.3}$$

where:

- ρ is the water density;

- S_{0B} is the mean wetted hull surface;

- **n** is the normal vector projection on the relevant degree of freedom.

As the STC is a moored structure, the second order effect has to be investigate in order to see its contribution on the response of the structure. Newman's approximation [35] has been chosen in order to estimate the slow-drift motions. This method allows to evaluate the second-order transfer function by knowing only the mean drift transfer function. In the MWL survival mode the second order forces are applied to the torus in order to consider the larger reflected waves generated [2].
For a moored structure slow-drift resonance oscillations occur in surge, sway and yaw.
According to Newman's approximation the second order transfer function for the difference frequency loads does not change very much when $\omega_i = \omega_j$ (ω_i, ω_j wave frequencies). That is why to solve the second-order transfer function only the first-order solution is needed. Furthermore, instead of calculating the slow-drift excitation force in a time series, it could be convenient to write it in a spectral form [35]. The low frequency part of the wave force spectrum is calculated according to Pinkster as:

$$S_F = 8 \int_0^\infty S(\omega)S(\omega + \mu)\left(\frac{\bar{F}_i(\omega + \mu/2)}{\zeta_a^2}\right)^2 d\omega \tag{1.4}$$

where,

- $\mu = \omega_i - \omega_j$;

- $S(\omega)$, $S(\omega + \mu)$ are the wave spectral values for ω and $\omega + \mu$;

- $\frac{\bar{F}_i(\omega+\mu/2)}{\zeta_a^2}$ is the mean drift force transfrer function. ζ_a represent the incoming wave amplitude.

The viscous forces on a slender body, as the one studied, have been expressed in terms of Morrison's equation as [2]:

$$\mathbf{F}_D = \frac{1}{2}\rho C_D A(\mathbf{V}_0 - \mathbf{V}_1)|\mathbf{V}_0 - \mathbf{V}_1| \tag{1.5}$$

where:

- A is the cross-section area of the slender element;

- C_D is the quadratic coefficient;

- V_0 is the incident wave velocity vector at the center of the element strip, perpendicular to the element in vertical direction;

- V_1 is the body motion velocity vector at the center of the element strip, perpendicular to the element in vertical direction.

Once integrated this equation for all the slender elements that combined define the STC, it is possible to define the total viscous force on the spar and on the torus.

While studying the behaviour of the STC in extreme conditions in the MWL survival mode it is important to remember that the torus is locked to the spar to prevent the relative motions. In the model tests load cells have been installed between the two structures in order to measure the the coupling forces. In the numerical modelling, the PTO stiffness coefficient K_{PTO} and the PTO damping coefficient D_{PTO} are set to very high values to prevent the relative motion between the two structures.

1.5.3 Equation of motions

When the hydrodynamic forces have been computed it is possible to set up the equations of rigid body motions. If the STC is considered as a rigid floating system with zero froward speed, the equation of motion, taking into account the first and second order weave and wind loads can be written in frequency domain [41] as:

$$-\omega^2(\mathbf{M} + \mathbf{A}(\omega))\mathbf{x}(\omega) + i\omega\mathbf{B}(\omega)\mathbf{x}(\omega) + \mathbf{R}\mathbf{x}(\omega) = \mathbf{F}(\omega) \qquad (1.6)$$

herein:

- ω is the wave frequency;

- $\mathbf{M}$ is the structural mass matrix;

- $\mathbf{A}(\omega)$ is the added mass matrix dependent from the frequency;

- $\mathbf{B}(\omega)$ is the radiation damping matrix dependent from the frequency;

- $\mathbf{R}(\omega)$ is the linear restoring force term considering buoyancy and gravity;

- $\mathbf{x}(\omega)$ is the motion vector;

- $\mathbf{F}(\omega)$ is the external force vector.
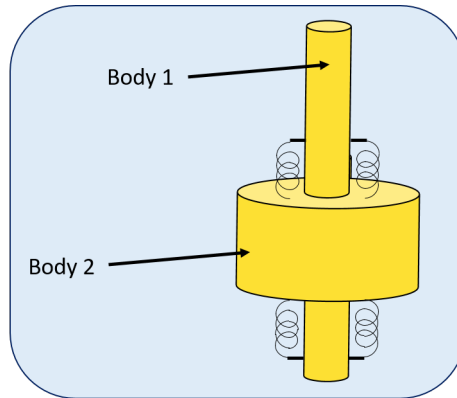
Figure 1.17: STC model composed by spar floater and torus.

Using the equation of motion in frequency domain the linear problem can be solved in an efficient way. For what it concern the study of the STC several terms are nonlinear as the viscous effect, the geometry and the mooring system and strongly nonlinear hydrodynamic forces acts on it, like the slamming and the nonlinear buoyancy and Froude-Krylov forces. In order to solve this problem is then necessary to introduce the equation of motion in time domain. For a single floating rigid body the equation of motion in time domain can be written as:

$$(\mathbf{M} + \mathbf{A}(\infty))\ddot{\mathbf{x}}(t) + \mathbf{C}\dot{\mathbf{x}}(t)|\dot{\mathbf{x}}(t)| + \int_0^t \mathbf{k}(t-\tau)\dot{\mathbf{x}}(\tau)d\tau + \mathbf{R}\mathbf{x}(t) = \mathbf{F}(t, x, \dot{x}) \quad (1.7)$$

where:

- $\mathbf{x}$ displacement vector in time domain;

- $\dot{\mathbf{x}}$ velocity vector in time domain;

- $\ddot{\mathbf{x}}$ acceleration vector in time domain;

- $\mathbf{A}(\infty)$ added mass matrix at infinite frequency;

- $\mathbf{C}$ is the quadratic viscous damping coefficients matrix;

- $\mathbf{F}(t, x, \dot{x})$ is the summation of external forces in time domain;

- $k(\tau)$ is the radiation impulse response function matrix due to the wave memory effects.

It should be noticed that the equation in frequency domain and time domain are not equivalent. Indeed in the time domain formulation viscous effect are considered and the external forces are also dependent from the position and velocity of the body while the external force vector is only dependent on the frequency in the frequency domain formulation. The convolution term can then be written as:

$$k(\tau) = \frac{2}{\pi} \int_0^\infty [\mathbf{B}(\omega) - \mathbf{B}(\infty)]cos(\omega t)d\omega = -\frac{2}{\pi} \int_0^\infty \omega[\mathbf{A}(\omega) - \mathbf{A}(\infty)]sin(\omega t)d\omega$$
$$(1.8)$$

where $\mathbf{B}(\infty)$ is the radiation damping matrix at infinite frequency, and in the case studied where the body has no forward speed, is zero.

Even if in this study the only condition of the STC that is going to be considered is the MWL survival condition, where the torus is locked to the spar, spar-torus interface forces are still present. That means that the equations of motion have to be rewritten to take into consideration the two bodies.

$$\begin{bmatrix} (\mathbf{M} + \mathbf{A}(\infty))_{11} & A(\infty)_{12} \\ A(\infty)_{21} & (\mathbf{M} + \mathbf{A}(\infty))_{22} \end{bmatrix} \begin{bmatrix} \ddot{\mathbf{x}}_1(t) \\ \ddot{\mathbf{x}}_2(t) \end{bmatrix} + \begin{bmatrix} \mathbf{C}_{11} & 0 \\ 0 & \mathbf{C}_{22} \end{bmatrix} \begin{bmatrix} \dot{\mathbf{x}}_1(t)|\dot{\mathbf{x}}_1(t)| \\ \dot{\mathbf{x}}_2(t)|\dot{\mathbf{x}}_2(t)| \end{bmatrix} +$$

$$+ \int_0^t \begin{bmatrix} \mathbf{k}_{11}(t-\tau) & \mathbf{k}_{12}(t-\tau) \\ \mathbf{k}_{21}(t-\tau) & \mathbf{k}_{22}(t-\tau) \end{bmatrix} \begin{bmatrix} \dot{\mathbf{x}}_1(\tau) \\ \dot{\mathbf{x}}_2(\tau) \end{bmatrix} d\tau + \begin{bmatrix} \mathbf{R}_{11} & \mathbf{R}_{12} \\ \mathbf{R}_{21} & \mathbf{R}_{22} \end{bmatrix} \begin{bmatrix} x_1(t) \\ x_2(t) \end{bmatrix} = \begin{bmatrix} \mathbf{F}_1(t, x, \dot{x}) \\ \mathbf{F}_2(t, x, \dot{x}) \end{bmatrix}$$

where 1 or 11 and 2 or 22 corresponds to the two bodies, the spar (1) and the torus (2).
Subscript 12 or 21 signifies coupling terms between the spar and the torus.

The external forces, represented by the term in the right hand side can be divided into:

- excitation forces: hydrodynamic forces, mooring line forces and current forces. All of these forces depends on the position and on the environmental conditions.

- coupling forces: spar-torus interface forces. These forces represents the coupling of the two bodies.

1.6 Previous studies

– Made Jaya Muliawan:
The main objective of his Doctoral thesis [30] was to study numerically the global responses of a two-body FWEC, an overtopping FWEC,and the STC, focusing on the mechanical couplings and on the mooring system. Muliawan compared the performance of the STC concept and the spar FWT in mild sea states. In operational conditions the behaviour of the STC resulted to be comparable to the spar FWT. Some issue, instead, have been founded in extreme conditions where the structural integrity in not guaranteed. For the study of the extreme conditions, Muliawan proposed several survival modes for the STC.

– Ling Wan:
In his Doctoral thesis [2] Wan investigated the integrated global performance of the STC concept and compared the numerical analysis with the model tests for both the functionality and survivability simulations. Being the survivability of the STC a weakness of the system, the numerical model for two of the survival modes proposed have been analyzed. The model test, performed in two different facilities, resulted to be close to the numerical model for the survival mode in which the torus is submerged (SUB) while several discrepancies have been founded for the second survival mode tested in which the torus is locked mechanically to the spar at the mean water level (MWL). In the MWL mode strongly nonlinear phenomena, caused by the water entry and exit of the torus together with green water and slamming, have been observed. To solve the strongly nonlinear hydrodynamic problems a nonlinear solver, proposed by Greco and Lugni [28], successfuly validated by Greco et al. [29], have been applied from Wan.

– Haobin Liu:
In his master thesis [32] Liu presents the results of a nonlinear stress analysis of the interface structure between the spar and the torus in the combined wind and wave energy concept (STC). Constant loadings have been applied to investigate the local interface model performance under different loading conditions. Different parameters for the interface design have been investigated performing sensitivity studies.

– Sevyllen Kistnen Appiah:
In the master thesis [31] Appiah analyzed numerically the unstable motions for regular and irregular wave conditions that have then be compared with the experimental tests. Appiah focused on Mathieu instability that occurs when the time period of the wave

excitation is equal to half of the natural period of the pitch motion and thus, pitch res-
onance develop. Mathieu instability occurs because the heave motion influences the
restoring term of the pitch motion which then varies in time. This phenomenon may
induce significant loads in the structural components which should be investigated.

1.7 Objectives and scope of the thesis

The main objective of this Thesis is to numerically and experimentally investigate the
performance of the STC concept under the mean water level (MWL) survival mode in a
comprehensive way.
The significant wave slamming loads on the bottom of the torus observed in extreme wave
conditions when the torus was fixed to the spar at the mean water level is numerically
analyzed using the SIMO code which is based on the linear potential theory. The code
for the MWL mode, provided a valid model for the regular wave cases with a small wave
height of 2 m and in small sea states when there was no water entry and exit of the torus but
resulted unreliable in regular wave cases with a wave height of 9 m and extreme sea states
when there was water entry and exit of the torus. Consequently, a simplified nonlinear
wave load model is develop and implement in SIMO considering:

- nonlinear buoyancy force

- nonlinear Froude-Krylov force

- simplified slamming force

1.8 Thesis Overview

The aim of this graduation thesis is to investigate the effects of nonlinear loads caused by
slamming on the spar torus combination (STC) concept. The thesis is organized in the
following way:

Chapter 1: Introduction. Describes the general background of this study and presents
the STC concept which is the structure studied in the whole Thesis. Furthermore in this
chapter the theoretical Background is presented. This section focuses on the basic theories
for studying the motion of the STC concept considering linear and nonlinear features.

Chapter 2: Slamming. Presents the slamming phenomena and the theory applied for the
study of this force for the STC concept in the MWL survival mode.

Chapter 3: Nonlinear buoyancy and nonlinear Froude-Krylov force. Nonlinear buoyancy
and nonlinear Froude-Krylov force are analyzed considering both the pressure integration
method and the approach proposed by Sclavounos in his study of "*Nonlinear impulse of
ocean waves on floating bodies*" [40].

Chapter 4: Experimental Results. Describes facility and structure of the model tests done

at MARINTEK and presents the results obtained for the survival mode in extreme wave conditions.

Chapter 5: Numerical analysis. Briefly explain SIMO code and shows the results of the numerical analysis done with SIMO considering the nonlinear loads. This chapter presents also the comparison of experimental and numerical results in cases with strongly nonlinear phenomena for the STC in the MWL survival mode.

Chapter 6: Conclusion, discussion and recommendations for future work. Presents the conclusions and discussions and provides recommendations for future work.

1.9   Thesis work flowchart

Chapter 2
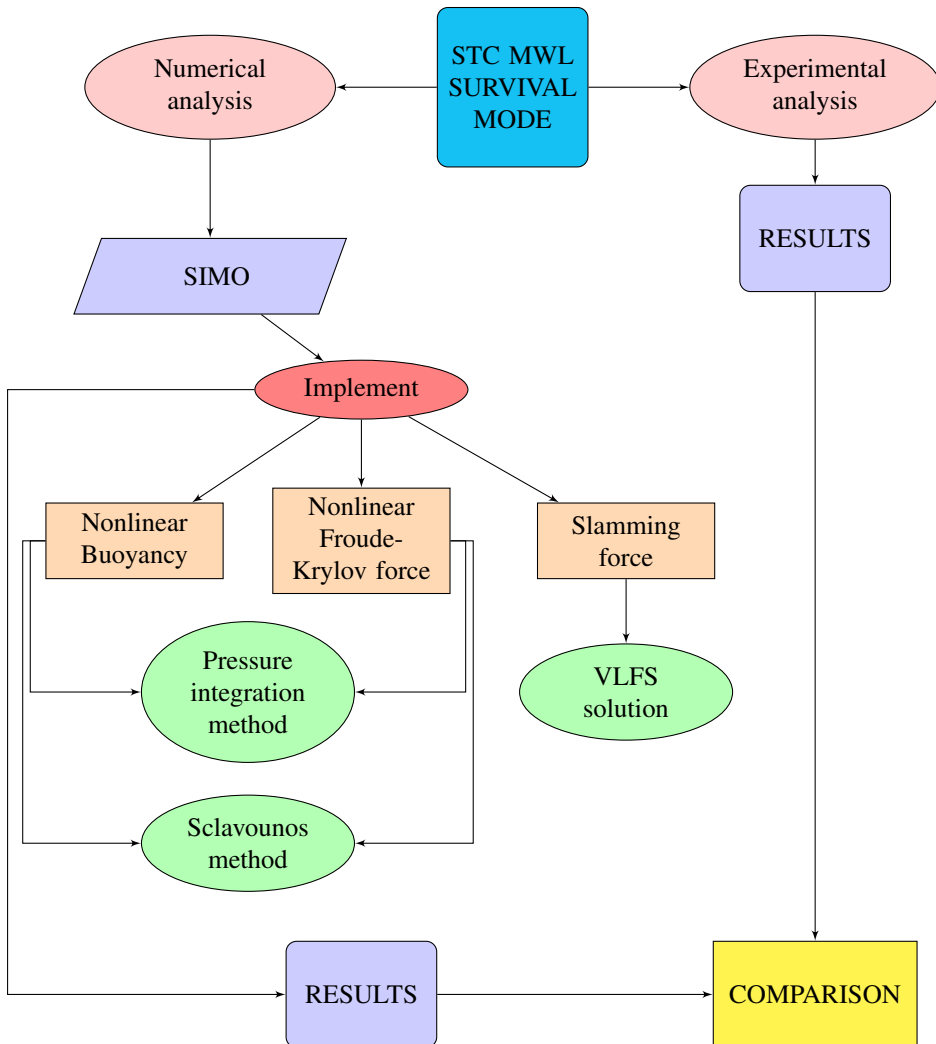
Slamming

2.1 Introduction

In this section the nonlinear phenomena, that has been observed on the torus under extreme sea state (e.g., Hs>6 m), is going to be introduced. The analysis of slamming load is necessary to ensure the integrity of the structure under extreme environmental conditions due to large wave forces on the torus. The study focus on the MWL survival mode, in which strongly water entry and exit (WEE) phenomena, accompanied with the green water shipped on the torus top and the wave impact on the torus bottom, have been observed [2]. The research will focus only in the vertical loads which resulted to be the most critical. But, as highlighted from Haobin Liu in his Master Thesis [32], is important to remember how the slamming under severe sea state increase also the force between spar and torus in the horizontal direction.

Slamming is caused by sudden retardation of a volume of fluid which causes a considerable force to act on the structure [33]. In other words slamming can be defined as an impulse load with high pressure peaks that occurs during the impact between a body and water. The duration of slamming pressure is of the order of milliseconds and it is very localized in space. This means that the spatial and time scales involved in the solution of the problem, are so small that can be seen as a perturbation of the flow variables nu-
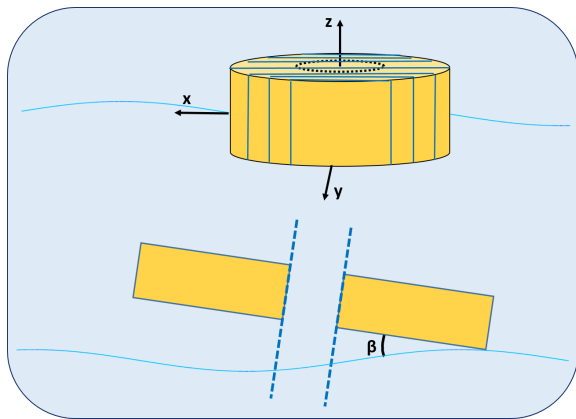
Figure 2.1: Body divided in strips with plane parallel to the xz plane and relative angle β in order from the top.

merically obtained at the impact instant [34]. Furthermore, the position where high slamming pressure occurs changes with time and depends on how the structure hits the water [35].

The non-linearity of the slamming phenomena has been extensively studied by Abramson at al. and presented in Liquid Slosh in LNG Carriers [36], where experimental results of the slamming pressure due to sloshing in tanks have been analyzed. The outcome of this study is that even if the tank is forced to oscillate harmonically the pressure is neither periodic nor harmonic. The pressure peaks varies from cycle to cycle and this is the evidence on how the slamming phenomena presents nonlinear problematic.

The impact on the bottom of the torus caused by the slamming are expected to start from the outer circle of the torus for long incident waves. The impact angle can be approximated to the relative angle between the instantaneous body position and the local slope of the incident wave in the direction of the wave. The problem has been solved applying the strip-theory approach in the local x-direction. For each strip, the local Wagner-type solution, derived by Faltinsen et al. [34] for the bottom slamming of a Very Large Floating Structure (VLFS), have been used. The main characteristic of Wagner method is that it accounts for the local up-rise of the water, while von Karman method neglect the spray effect, hence the wetted surface length is smaller [37].

2.1.1 Wagner's slamming model

Wagner slamming model assumes a local small angle β [38]. This model can be used to asses the space-averaged pressures that matters for structural stresses [37].

For the purpose of this work, only the outer flow domain, shown in Figure 2.2, is described. The intersection between the free surface and the body surface, within the outer flow domain, is very close to the spray root. As shown in Figure 2.2, $V_0 \cdot t$ corresponds to the submergence of the lowest point of the structure relative to the calm water surface. However, as shown in Figure 2.2, the impact cause the up-rise of the water.

At each time instant the boundary value problem, shown in Figure 2.3, have to be solved. Being the angle (β) small ($0° < \beta < 4°$), the body boundary condition re-
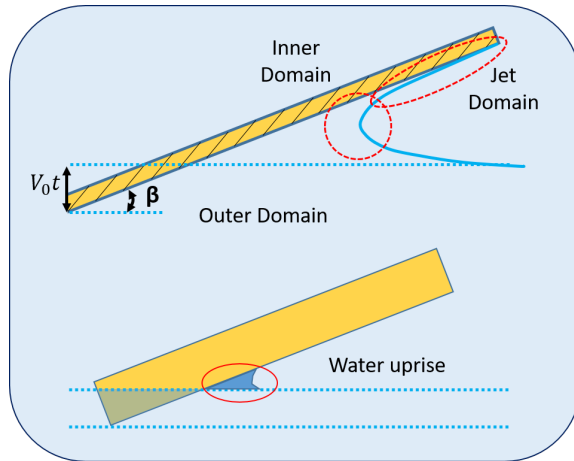
Figure 2.2: Definition of outer, inner and jetflow domain on the top. Uprise of the water caused by the impact on the bottom.

quires that no flow through the body surface is transferred to a straight line between -c(t) ant c(t) using Taylor expansion. Furthermore, in Figure 2.3, is possible to notice that the free-surface condition $\varphi = 0$ at z=0 is used, considering that, during the impact, the fluid accelerations in the vicinity of the body dominate over gravitational acceleration.

The solution of the boundary value problem, shown in Figure 2.3, is given from the complex velocity potential [39]:

$$\Phi = \varphi + i\psi = iV_0 Z - iV_0(Z^2 - c^2)^{1/2} \tag{2.1}$$

where, Z=x+iz is a complex variable, φ is the velocity potential and ψ is the stream function.
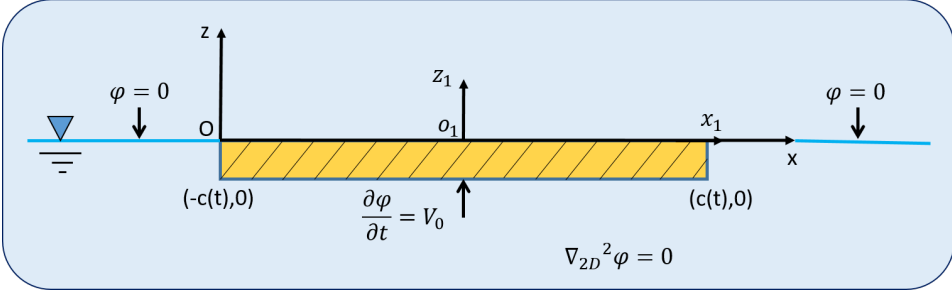
Figure 2.3: Boundary-value problem for the velocity potential φ in the analysis of the impact between a two-dimensional body and the water.

Knowing the complex velocity potential is then possible to derive the complex velocity as:

$$\frac{d\Phi}{dZ} = u - iw = iV_0 - iV_0 \frac{Z}{(Z^2 - c^2)^{1/2}} \tag{2.2}$$

Equation 2.2, considering the boundary conditions and the underside of the body $z=0^-$, gives:

$$\Phi = \varphi + i\psi = iV_0 x - V_0(c^2 - x^2)^{1/2} \qquad for \ |x| < c, \ z = 0^- \tag{2.3}$$

which means that the velocity potential on the body can be written as:

$$\varphi = -V_0(c^2 - x^2)^{1/2} \qquad for \ |x| < c, \tag{2.4}$$

2.1.2 Application of Wagner's model to the STC

The shallow draft of the torus implies that slamming will occur in wave conditions where the water is shipped on deck. Furthermore, the angle between the free surface and the bottom is smaller than $5°$ and very rapid changes of the wetted area close to the edge occur.

For a body with a horizontal flat bottom that hits the free-surface,
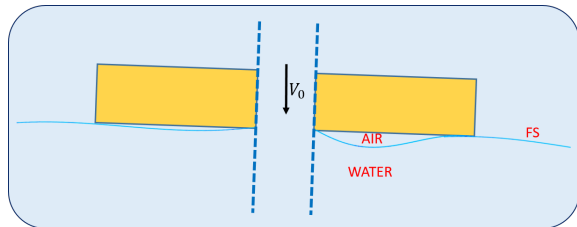
Figure 2.4: Formation of an air pocket during entry of a body with a horizontal flat bottom.

as the one shown in Figure 2.4, it can be noticed an initial phase identify by the formation of a compressible air pocket between the body and the free-surface. In order to take into account the effect of the air cushions, the airflow is neglected and the cavity pressure related to the cavity volume is modelled by an adiabatic relationship:

$$p = p_a \left[\frac{Vol_0}{Vol(t)} \right]^\gamma \tag{2.5}$$

Herein,

- p_a is the atmospheric pressure;

- Vol_0 is the initial volume at closure of the air cushion;

- $\gamma = 1.4$ treating the air as an ideal gas.

In order to analyze the problem it is important to notice that close to the first impact location, the water free surface can be approximated by a straight line. Furthermore is going to be assumed that the involved spatial and time scales are so small that the local solution can be approximated as a perturbation of the flow variables numerically obtained at the impact instant. Finally the possibility that on the front side of the structure air cavities of the type shown in water-shipping phenomena are formed is neglected.

The vertical velocity of the body, V_0, before the impact is supposed to be constant. The flow due to the impact is then solved in the same way Wagner did for two-dimensional impact of a rigid body on an initially calm free surface. Differently from Wagner' solution, it is assumed that the body-free surface intersection point (x=0) does not change.

The following section presents the local analytical solution for the slamming load of the STC.

2.2 Wave impact on the torus

In coordinate system $x_1 o_1 z_1$, the velocity potential Φ on the wetted body surface according to equation 2.2 is:

$$\Phi = -V_0(c^2 - x_1^2)^{1/2} \qquad |x_1| < c(t) \tag{2.6}$$

From the solution of the boundary value problem, it follows

$$\frac{\partial \Phi}{\partial z} = \frac{V_0|x_1|}{\sqrt{x_1^2 - c^2(t)}} - V_0 \qquad on \ z = 0, \ |x_1| > c(t) \tag{2.7}$$

and

$$W_R = \frac{\partial \Phi}{\partial z} + V_0 = \frac{V_0|x_1|}{\sqrt{x_1^2 - c^2(t)}} - V_0 \qquad on \ z = 0, \ |x_1| > c(t) \tag{2.8}$$

herein, W_R is the relative vertical velocity between the fluid particles on the free surface and the body.
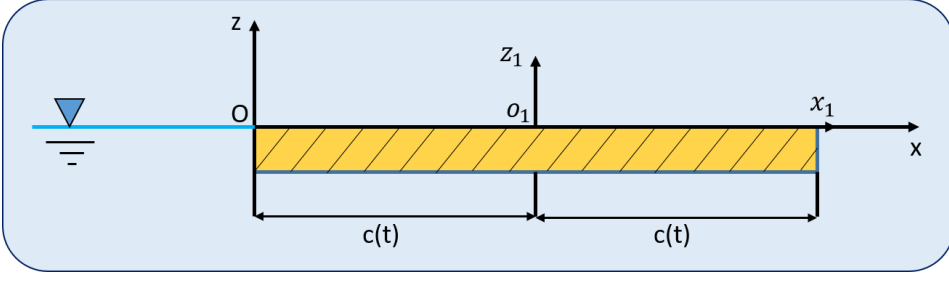
Figure 2.5: Two coordinate systems at the front of a wetdeck.

The relation between the coordinates xoz and the coordinates $x_1 o_1 z_1$ is

$$\begin{cases} x = x_1 + c \\ z = z_1 \end{cases} \tag{2.9}$$

Then we can obtain the reformation of equations 2.6, 2.7, 2.8 in coordinate system xoz as

$$\Phi = -V_0\sqrt{c^2 - (x-c)^2} = -V_0\sqrt{x(2c-x)} \qquad 0 < x < 2c(t) \tag{2.10}$$

$$\frac{\partial \Phi}{\partial z} = \frac{V_0|x-c|}{\sqrt{(x-c)^2 - c^2}} - V_0 = \frac{V_0|x-c|}{\sqrt{x^2 - 2cx}} - V_0 \quad on\ z = 0,\ x < 0\ or\ x > 2c(t) \tag{2.11}$$

$$W_R = \frac{V_0|x-c|}{\sqrt{x^2 - 2cx}} \qquad on\ z = 0,\ x < 0\ or\ x > 2c(t) \tag{2.12}$$

Focusing on one fluid particle with a given x-coordinate, at time instant t, this particle intersecting the body surface, then the distance during this time period that the particle moves is

$$\eta_b(x) = \int_0^t \frac{V_0|x-c|}{\sqrt{x^2 - 2cx}} dt \tag{2.13}$$

here t=0 corresponds to initial impact and $\eta_b(x)$ is a known function which is

$$\eta_b(x) = xtan\beta \tag{2.14}$$

Equation 2.13 is an integral equation that determines c(t), then let

$$\mu(c)dc = V_0dt \tag{2.15}$$

The moving intersection on the right is considered, so (x-c) is positive, then equation 2.13 can be reformed as

$$\eta_b(x) = \int_0^t \frac{V_0|x-c|}{\sqrt{x^2 - 2cx}} dt = \int_0^{\frac{x}{2}} \frac{(V_0dt)|x-c|}{\sqrt{x^2 - 2cx}} = \int_0^{\frac{x}{2}} \frac{\mu(c)(x-c)}{\sqrt{x^2 - 2cx}} dc \tag{2.16}$$

To find an approximate solution of equation 2.16, we can assume that

$$\mu(c) \approx A_0 + A_1 c \tag{2.17}$$

Then

$$\eta_b(x) \approx \int_0^{\frac{x}{2}} \frac{(A_0 + A_1 c)(x - c)}{\sqrt{x^2 - 2cx}} dc = \frac{2}{3} A_0 x + \frac{1}{5} A_1 x^2 \tag{2.18}$$

From equations 2.14 and 2.18, it follows

$$x tan\beta = \frac{2}{3} A_0 x + \frac{1}{5} A_1 x^2 \quad \Rightarrow \quad \begin{cases} A_0 = \frac{3}{2} tan\beta \\ A_1 = 0 \end{cases} \tag{2.19}$$

From equation 2.15, it follows

$$\frac{3}{2} tan\beta dc = V_0 dt \tag{2.20}$$

Integrate both side of the above equation, it gives

$$\int_0^c \left(\frac{3}{2} tan\beta \right) dc = \int_0^t V_0 dt \quad \Rightarrow \quad c(t) = \frac{2V_0 t}{3tan\beta} \tag{2.21}$$

where t=0 corresponds to initial impact.

Using the velocity potential defined in equation 2.10 define the impact pressure and the vertical force on the wetdeck:

$$p = -\rho \frac{\partial \Phi}{\partial t} = -\rho \frac{\partial}{\partial t} \left[-V_0 \sqrt{x \left(-x + \frac{4V_0 tx}{3tan\beta} \right)} \right] = \frac{2\rho V_0^2 x}{3tan\beta} \cdot \frac{1}{\sqrt{x \left(-x + \frac{4V_0 tx}{3tan\beta} \right)}} \tag{2.22}$$

Finally the 2D vertical force acting on the impacting body at time instant t can be expressed as

$$F_3 = \int_0^{2c} p dx = \int_0^{2c} \frac{2\rho V_0^2 x}{3tan\beta} \cdot \frac{1}{\sqrt{x \left(-x + \frac{4V_0 tx}{3tan\beta} \right)}} dx = \frac{2\rho V_0^2}{3tan\beta} \int_0^{2c} \frac{x}{\sqrt{-x^2 + 2cx}} dx \tag{2.23}$$

Let

$$x = c + c\,cos\theta \quad \theta \in [0, \pi] \quad \Rightarrow \quad dx = -c\,sin\theta d\theta \tag{2.24}$$

Then from equation 2.25 the vertical force is

$$F_3 = -\frac{2\rho V_0^2}{3tan\beta} \int_\pi^0 \frac{c(c + c\,cos\theta)sin\theta}{\sqrt{-(c + c\,cos\theta)^2 + 2c(c + c\,cos\theta)}} d\theta = \frac{2\rho V_0^2 c\pi}{3tan\beta} = \frac{4\rho \pi V_0^3 t}{9tan^2\beta} \tag{2.25}$$

In this analysis gravity have been neglected which means that the generation of surface waves as well as the Froude-Krylov and hydrostatic force are disregarded. The latter two forces are introduced and explained in the next chapter. Being the impact angle between the structure and the free surface small, the nonlinear Froude-Krylov and hydrostatic force results to be important relative to the slamming forces [37].

2.3   Computation of the Slamming force in MATLAB

In order to compute the slamming force on the bottom of the torus, the procedure explained in the previous section have been applied for the torus in MATLAB. Once the slamming model have been implemented the results have been compared to the experimental results before writing a Dynamic-Link-Library (DLL) in FORTRAN which is necessary to add to the equation of motions in SIMO the slamming loads.
The first step of the calculation has been to determine the initial and the final time for each strip. The strips have been divided in three different categories, as shown in Figure 2.6 and Figure 2.7:

- central strip

- "divided" strips

- "entire" strips
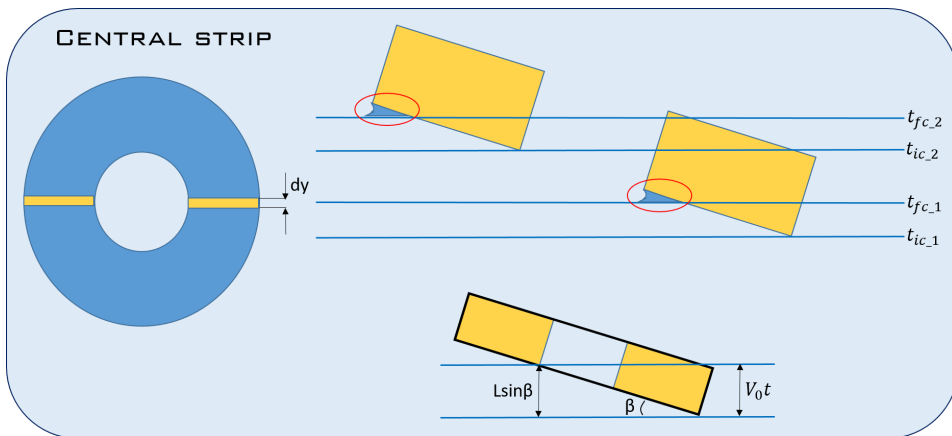
Figure 2.6: Torus central strip.

The impact time is defined as the point where the bottom of the torus touch the water surface. In order to find this impact time the shallow-water approximation, being the waves long in the studied cases, is considered. This means that even if the slamming will start from the outer diameter of the torus, the time of the slamming impact is approximated to the time in which the central point of the bottom of the torus touch the water. Other assumptions, as previously explained, are the relative angle and the vertical velocity which

are considered to be constant during the slamming phenomena. Furthermore, while studying the slamming loads on the STC it has been chosen to not consider the effect of the spar but to study the torus as if it was a single body.

After have determined the impact instant, the slamming force have been founded integrating on time the force for each strip. The initial time is different for each strip and has been calculated through the geometrical consideration, shown in Figure 2.6 so that:

$$Lsin\beta = V_0 t \quad \Rightarrow \quad t = \frac{Lsin\beta}{V_0} \tag{2.26}$$

while the final time have been founded considering the watted surface due to the spray effect, as explained in the previous section:

$$2c = \frac{4V_0 t}{3tan\beta} \quad \Rightarrow \quad t = \frac{3(2c)tan\beta}{4V_0} \tag{2.27}$$
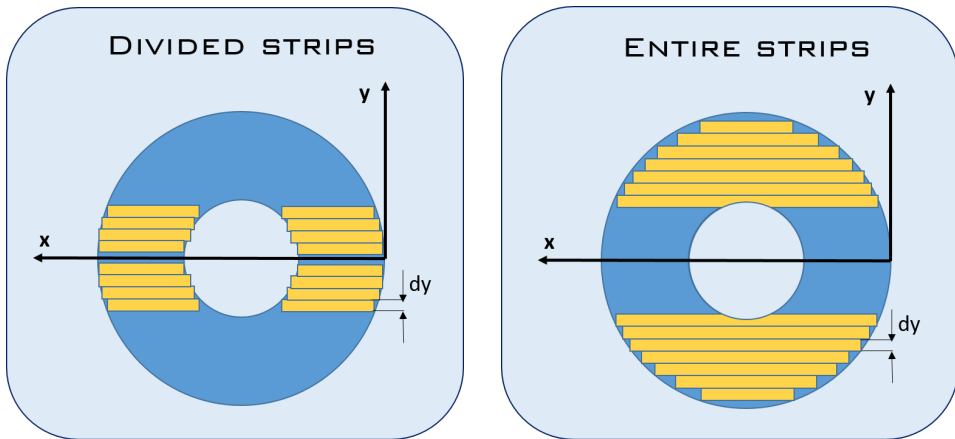
Figure 2.7: Torus "divided" and "entire" strips.

Finally, as shown in Figure 2.8 the sum of the forces acting on the three different type of strips have been summed to obtain the slamming loads acting on the torus at each time step.

In Figure 2.9 the results for the three different type of strips id presented, while in Figure 2.10 the total slamming force is plotted.
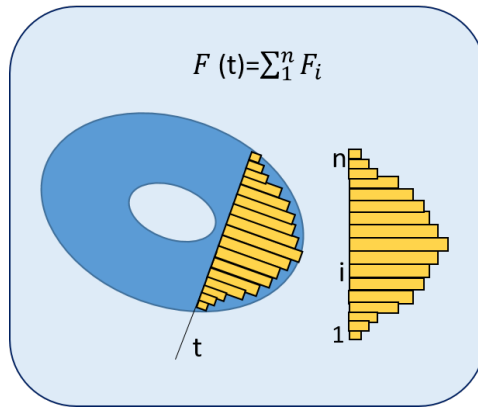
Figure 2.8: Summation of the slamming force on each strip.

In Figure 2.9 it can be clearly seen that the influence of the spar is not considered. That explain why the force drops to zero. The strip on the right and on the left of the spar, under this assumption, have been considered to be independent. Moreover, it is possible to notice that the value of the two peaks of the central strip is the same, while for the "divided" strips the second peak presents a lower magnitude. This behaviour can be explained considering that the diameter of the spar is smaller than the diameter of the torus so the strips will touch the water at different times. Faster for the strip that touch first the water and slower for the strips after the spar, as it can be see from the curve at 0.05 s.
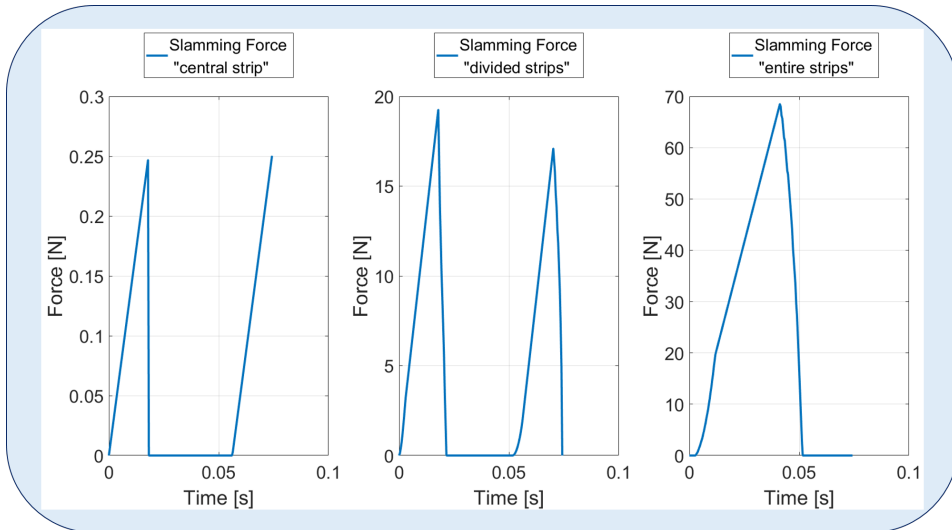
Figure 2.9: Slamming force on the central, divided and entire strips considering $V_0 = 0.2$ m/s and $\beta = 2.3°$.

The plot of the slamming force on the "entire" strips shows how this part of the torus presents the highest values. This result would be different if the affection of the spar is considered.

From the sum of the forces, presented in Figure 2.10 , it can be notice that the slamming of the structure is not symmetric. As explained before, this behaviour is due to the difference between diameter of the spar and of the torus.
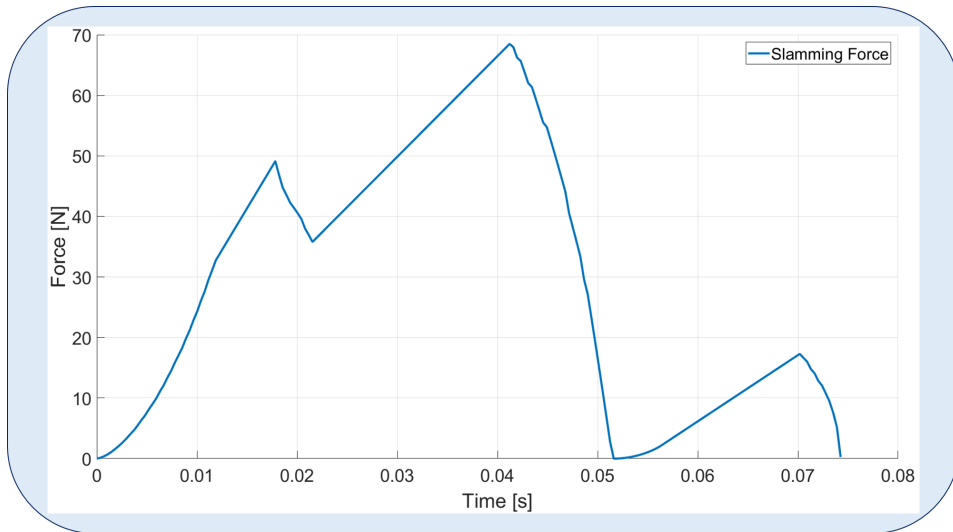
Figure 2.10: Total slamming force on the torus considering $V_0 = 0.2$ m/s and $\beta = 2.3°$.

Chapter 3

Nonlinear buoyancy and nonlinear Froude-Krylov forces

3.1 Pressure integration method

3.1.1 Calculation of forces with body at mean water level

The response of the STC is calculated for regular long crested deep water waves. Being the wave very long compared to the diameter of the torus, for the estimation of both the nonlinear buoyancy and the nonlinear Froude-Krylov forces, the shallow-water approximation is considered.
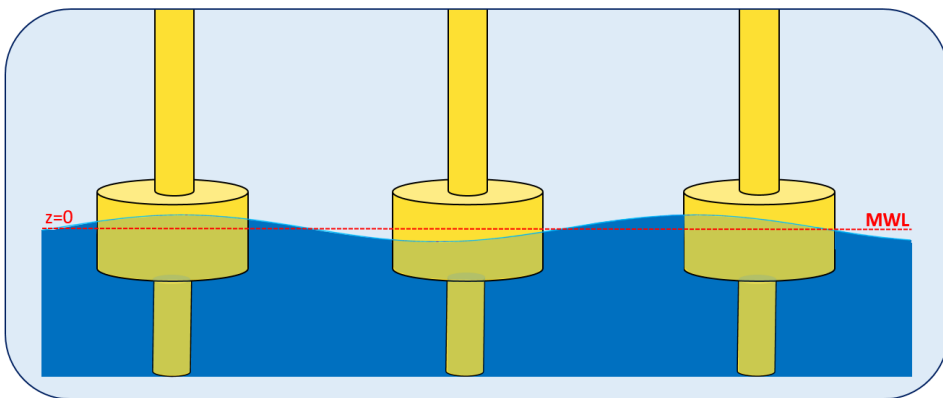
Figure 3.1: Torus at the mwl position for the calculation of the hydrostatic and Froude-Krylov forces.

The linear wave theory according to Faltinsen [35] has been used in order to determine the nonlinear loads on the STC. As the linear forces are already computed in SIMO, is

necessary to add only the nonlinear part, so the difference between the linear and nonlinear loads. Nonlinear forces are caused by the heave motion of the torus which on the analyzed conditions passes from being totally submerged to be completely out of the water.

The first step have been to calculate the loads for the torus at mean water level which is close to the linear case. The linear free surface is described by the z-coordinate as z=0 and the floater, while calculating the forces, is supposed to be in the mean water level position, as shown in Figure 3.1. As already pointed out, the approximation of using the mean position of the torus, is reasonable being the waves long. Indeed studying long waves means that the depth variation of the velocities and the dynamic pressure which varies according to e^{kz} is small. Herein, k is the wave number and z is the coordinate system with zero value at the mean free surface and negative downwards. Froude-Krylov and hydrostatic forces are calculated according to the linear theory.

After the calculation of the forces for the case with the torus at mean water level, the nonlinear time and space dependent hydrostatic and Froude-Krylov pressure forces are studied. According to this second approach, the time dependent position of the torus and the time dependent wave elevation are considered, as shown in Figure 3.2. Also in this second case hydrostatic and dynamic pressure are calculated using the linear wave theory, but the forces are found by integrating the pressures over the exact wetted surface at each time step [42].
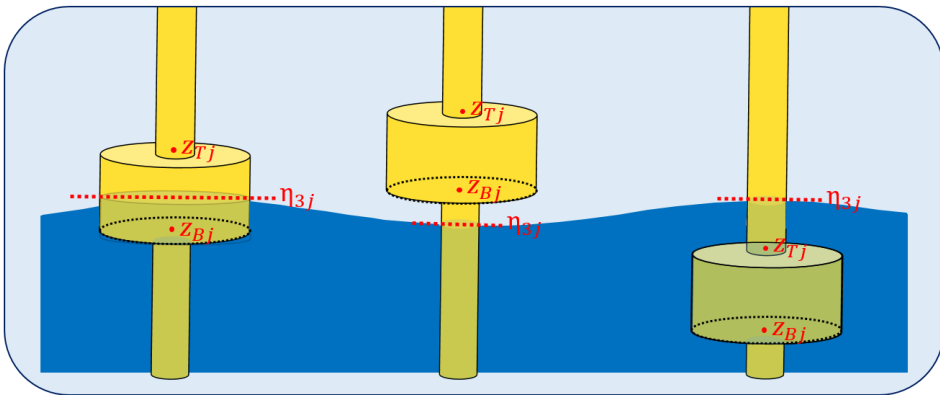
Figure 3.2: Torus and wave elevation different at each time step for the calculation of the nonlinear hydrostatic and Froude-Krylov pressure forces.

Even if the pressures according to this approach are calculated using the linear theory, the procedure will be referred to the nonlinear buoyancy and Froude-Krylov forces.

The general formulation of the pressure comes from Bernoulli equation [43]:

$$p - p_a = -\rho g z - \rho \frac{\partial \Phi}{\partial t} - \frac{1}{2}\rho|\nabla\Phi|^2 \tag{3.1}$$

where:

- p_a is the ambient pressure;

- ρ is the water density;

- Φ is the velocity potentialfor regular sinusoidal propagating waves on infinite water depth according to the linear theory [35]:

$$\Phi = \frac{g\zeta_a}{\omega}e^{kz}cos(\omega t - kx) \tag{3.2}$$

herein,

  - ω is the circular frequency: $\omega = 2\pi/T$;
  - k is the wave number: $k = 2\pi/\lambda$;
  - T is the wave period;
  - λ is the wave length: $lambda = (g/2\pi)T^2$;
  - ζ_a is the wave amplitude;
  - g is the acceleration of gravity;
  - t is the time variable;
  - x is the direction of wave propagation;
  - z is the vertical coordinate.

In equation 3.1 the first term represents the linear hydrostatic pressure, the second term is the dynamic pressure linear part while the third terms represents the quadratic part of the dynamic pressure.

Under the assumptions of inviscid fluid, according to the linear potential theory, the forces and moments are obtained by integrating the pressure along the wetted surface of the body [43].
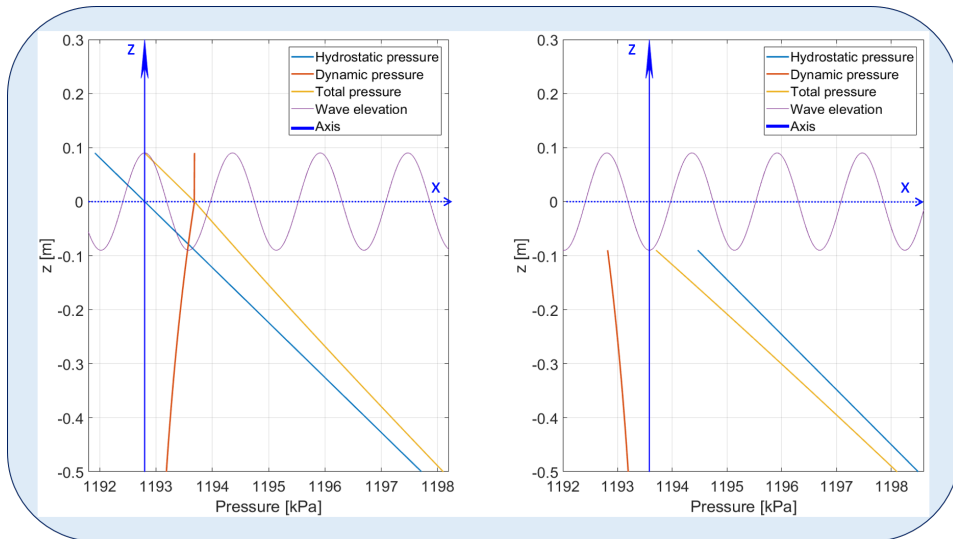
Figure 3.3: Linear hydrostatic, dynamic and total pressure underneath a wave crest and a wave trough in order from the left. The figure is based on a similar figure in [35].

The linear Froude-Krylov force is obtained integrating the linear part of the dynamic pressure according to the following equation:

$$p_{dyn} = \rho g \zeta_a e^{kz} sin(\omega t - kx) \tag{3.3}$$

where x is considered to be equal to zero considering the shallow-water approximation. The hydrostatic pressure is evaluated with the formula:

$$p_{hyd} = -\rho g z \tag{3.4}$$

The linear pressure behaviour according to linear theory is presented in Figure 3.3. From the figure it can be notice that the dynamic pressure is negative under a wave trough while is positive under the wave crest. Furthermore is important to remember that the linear theory assumes the velocity potential to be constant from the mean free-surface to the free-surface level [35].

The figure shows also the linear behaviour of the hydrostatic pressure with respect to z. The hydrostatic pressure is negative above the mean free surface and positive below it.

Being the pressure given relative to the atmospheric pressure means that it goes to zero at the free surface, so the static and dynamic contributions must balance each other [43]. As it can be seen in the left part of the figure this is exactly satisfied at a crest but not at a trough, where a higher-order error appears using the linear solution. Higher order error means that the error is proportional to ζ_a^n with an order $n \geq 2$.
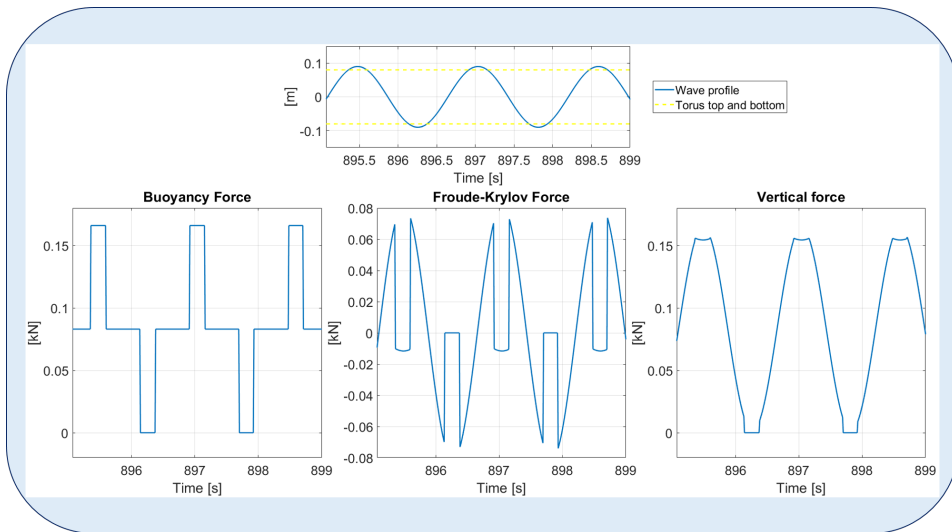
Figure 3.4: Nonlinear buoyancy and Froude-Krylov forces acting on the torus for the case with H=9 m and T=11 s and body at mean water level calculated applying the pressure integration method.

Once the pressure distribution is known for each point of the domain, considering that the torus is always at mean water level the pressure have been integrated over the top and

bottom surfaces depending from the wave elevation at each time step.

$$\mathbf{F} = \int_S p\mathbf{n}dS \tag{3.5}$$

Figure 3.4 shows buoyancy, Froude-Krylov forces and the sum of the two contribution for the case with the body at mean water level. It can be notice that the dynamic pressure have a really spiky behaviour but the sum of the two contributions is more regular. Also because of the strange behaviour of the dynamic pressure it has been chosen to compare this calculation with another model, later presented, to prove the consistency of the results. The accuracy of this solution could be higher considering Wheeler stretching, which is presented in Figure 3.5. But for comparing the results with another method for calculating buoyancy and Froude-Krylov force, explained in the next section, this approach has not been chosen.

Wheeler stretching method is based on the observation that the fluid velocity at the still water level is reduced compared with linear theory [33]. When applying this model, the pressure distribution is calculated as explained before until free surface. But, instead of considering the pressure constant above the free surface, the vertical coordinate is stretched up to the free surface elevation.
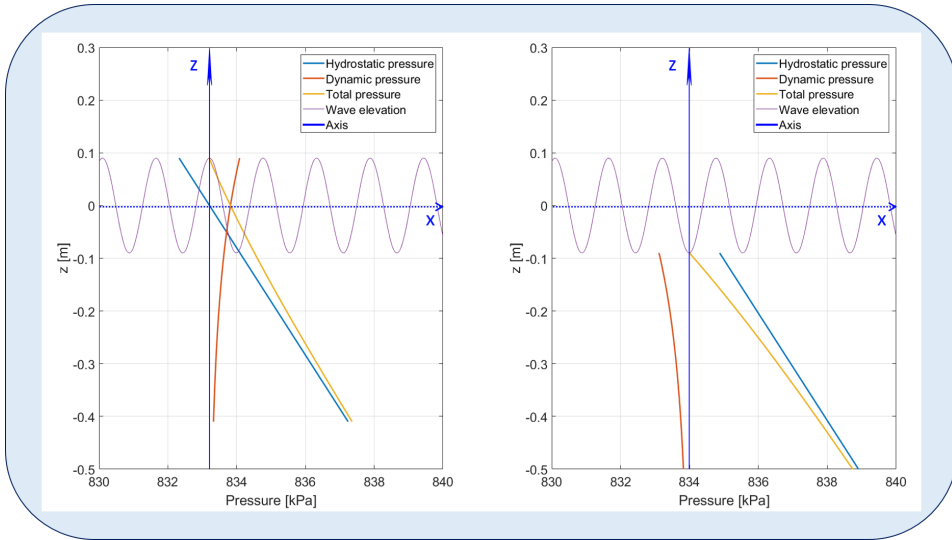
Figure 3.5: Linear hydrostatic, dynamic and total pressure underneath a wave crest and a wave trough considering the Wheeler stretching approach in order from the left.

3.1.2 Calculation of Nonlinear Forces

Hydrostatic and dynamic pressure have been calculated according to the linear wave theory, but the combination of the variation of the wetted surface with the motion of the torus will give rise to nonlinear excitation forces [42].

The nonlinear Froude-Krylov force is obtained integrating the linear part of the dynamic pressure according to the following equation:

$$p_{dyn} = \rho g \zeta_a e^{kz'} sin(\omega t - kx')$$ (3.6)

where x' is considered to be equal to zero considering the shallow-water approximation and z' is the actual vertical position of the bottom and of the top of the torus.
The hydrostatic pressure is evaluated with the formula:

$$p_{hyd} = -\rho g z'$$ (3.7)

The nonlinear forces are plotted in Figure 3.6 where it can be seen a that also in this case the dynamic pressure curve presents several peaks.
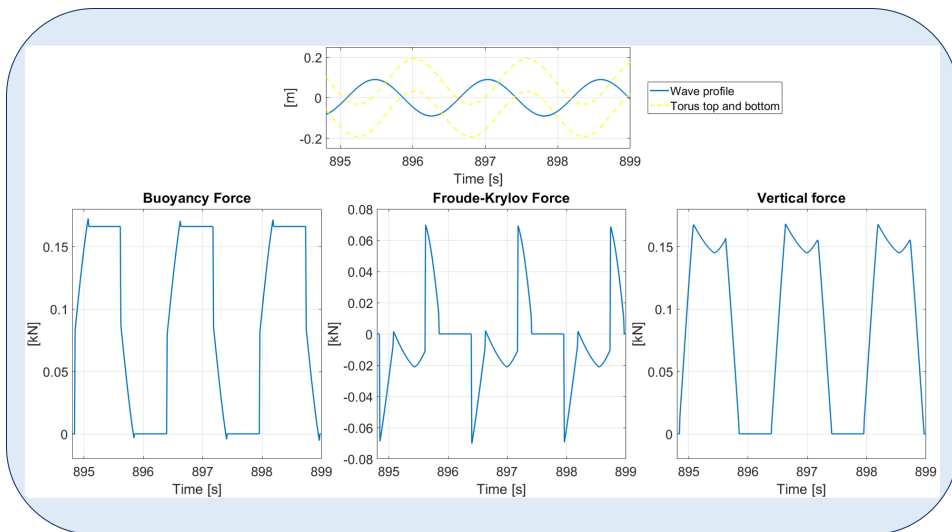
Figure 3.6: Nonlinear buoyancy and Froude-Krylov forces acting on the torus for the case with H=9 m and T=11 s calculated applying the pressure integration method.

3.2 Sclavounos method

This section presents the new formulation of the nonlinear loads exerted on floating bodies propose by Paul D. Sclavounos [40]. The application of this method saves computational time, indeed, forces and moments are calculated deriving in time the fluid impulse, while in the traditional approach the terms of Bernoulli's equation are derived in time and space. The application of this method leads to the generalized equations of motions for a rigid body in an ideal fluid.
Sclavounos formulation consider the nonlinear loads exerted by steep irregular surface waves on floating bodies in time domain. Instead of applying the momentum conservation principle, that for this kind of waves does not result consistent, Bernoulli's equation is

used to obtain the hydrodynamic pressure acting on the instantaneous body wetted surface. Knowing the hydrodynamic pressure is then possible to integrate it over the wetted surface and determine force and moment.

In order to model the irregular ambient waves with large amplitude the linear potential theory is applied considering a perturbation or a nonlinear method. Furthermore, also the radiation and diffraction wave disturbances caused by the floating body are studied with the potential flow theory.

As shown later, the nonlinear wave force acting on the body is founded to be the sum of the nonlinear hydrostatic force to the time derivative of the Froude-Krylov and radiation-diffraction impulses. In this formulation the viscous effects are neglected.
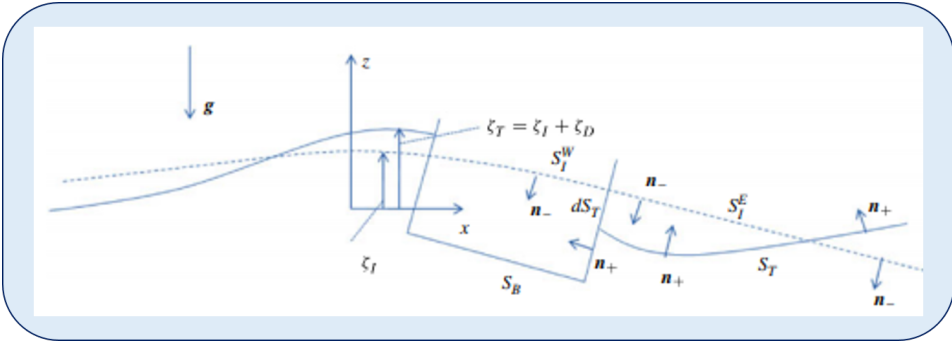
Figure 3.7: Body boundary in the center of the figure, fully nonlinear free surface (solid curves) and ambient wave surface (dashed curve). The ambient wave surface does not consider the disturbances caused by radiation and diffraction [40].

In Figure 3.7 is presented the boundary value problem. The floating body interacts with a nonlinear irregular ambient wave. The origin of the coordinate system XYZ is fixed on the calm water surface.

The main steps to derive equation 3.19, which define the exact nonlinear forces acting on the floating body, are going to be explained. The total velocity potential $\varphi(X, Y, Z, t)$ satisfies the following conditions:

- Laplace equation:

$$\frac{\partial^2 \varphi}{\partial X^2} + \frac{\partial^2 \varphi}{\partial Y^2} + \frac{\partial^2 \varphi}{\partial Z^2} = 0 \tag{3.8}$$

- the normal velocity of the total potential on the body boundary is equal to the normal velocity of the body boundary U_n:

$$\frac{\partial \varphi}{\partial n} = U_n \quad on \ S_B(t) \tag{3.9}$$

- the total velocity potential satisfies the nonlinear free-surface condition on the non-linear free surface Z=$\zeta_T(X, Y, t)$:

$$\left(\frac{\partial^2 \varphi}{\partial t^2} + g \frac{\partial \varphi}{\partial Z} + 2 \nabla \varphi \cdot \nabla \frac{\partial \varphi}{\partial t} + \frac{1}{2} \nabla \varphi \cdot \nabla (\nabla \varphi \cdot \nabla \varphi \cdot) \right)_{Z=\zeta_T(X,Y,t)} = 0 \tag{3.10}$$

$$\zeta_T(X, Y, t) = -\frac{1}{g}\Big(\frac{\partial\varphi}{\partial t} + \frac{1}{2}\nabla\varphi\cdot\nabla\varphi\Big)_{Z=\zeta_T(X,Y,t)} \tag{3.11}$$

condition that is satisfied also from the ambient wave potential φ_I

To find the hydrodynamic forces, the hydrodynamic pressure obtained from Bernoulli's equation is integrated over the instantaneous body wetted surface $S_B(t)$:

$$\mathbf{F}(t) = -\rho\int_{S_B(t)}\Big(\frac{\partial\varphi}{\partial t} + \frac{1}{2}\nabla\varphi\cdot\nabla\varphi + gZ\Big)\mathbf{n}ds \tag{3.12}$$

An important assumption of Sclavounos method is that at large distance from the radiation-diffraction waves vanish.

Applying the transport theorem on the fluid volume enclosed by the nonlinear free surface, V(t):

$$\frac{d}{dt}\int\int_{V(t)}\nabla\varphi\,dv = \int\int_{V(t)}\frac{\partial}{\partial t}\nabla\varphi\,dv + \int_{S(t)}\nabla\varphi\frac{\partial\varphi}{\partial n}ds \tag{3.13}$$

where S(t) is the control surface in which are contained the ambient wave and the body-induced radiation and diffraction wave disturbances.

Applying Gauss's theorem on the first term on the LHS of equation 3.13 and on the first term on the RHS:

$$\frac{d}{dt}\int_{S(t)}\varphi\mathbf{n}ds = \int_{S(t)}\Big[\frac{\partial\varphi}{\partial t}\mathbf{n} + \nabla\varphi\frac{\partial\varphi}{\partial n}\Big]ds \tag{3.14}$$

if then the quadratic term in Bernoulli's equation are added:

$$\int_{S(t)}\Big[\frac{\partial\varphi}{\partial t} + \frac{1}{2\nabla\varphi\cdot\nabla\varphi}\Big]\mathbf{n}ds = \frac{d}{dt}\int_{S(t)}\varphi\mathbf{n}ds - \int_{S(t)}\Big[\nabla\varphi\frac{\partial\varphi}{\partial n} - \frac{1}{2}\nabla\varphi\cdot\nabla\varphi\mathbf{n}\Big]ds \tag{3.15}$$

and considering that

$$\int_{S(t)}\Big[\nabla\varphi\frac{\partial\varphi}{\partial n} - \frac{1}{2}\nabla\varphi\cdot\nabla\varphi\mathbf{n}\Big]ds = 0 \tag{3.16}$$

is valid for any velocity potential over a close surface S(t), it is possible to write

$$\int_{S_B(t)}\Big[\frac{\partial\varphi}{\partial t} + \frac{1}{2\nabla\varphi\cdot\nabla\varphi} + gZ\Big]\mathbf{n}ds = \frac{d}{dt}\int_{S_B(t)+S_T(t)}\varphi\mathbf{n}ds + g\int_{S_B(t)+S_T(t)}Z\mathbf{n}ds \tag{3.17}$$

herein,

- $S_B(t)$ is the instantaneous wetted surface;

- $S_T(t)$ is the nonlinear free surface exterior to the body where the hydrodynamic pressure vanishes.

If then the body is considered as a point, with no displacement, equation 3.17 becomes:

$$0 = \frac{d}{dt}\int_{S_I(t)}\varphi_I\mathbf{n}ds + g\int_{S_I(t)}Z\mathbf{n}ds \tag{3.18}$$

where φ_I is the ambient wave velocity potential ($\varphi = \varphi_I + \varphi_D$) and $S_I(t)$ is the free surface of the ambient wave without the body. Equation 3.18 is the free-surface condition. The meaning of the equation is the integral balance between inertial and restoring effects. Now, taking the difference between Equation 3.17 and Equation 3.18, multiplying by $-\rho$ and considering the ambient wave surface inside the body (S_I^W) and its surface outside the body, applying Gauss's theorem and making some rearrangements it is possible to arrive to the final expression founded by Sclavounos to describe the nonlinear force acting on the body:

$$
\begin{aligned}
\mathbf{F}_B(t) = & -\rho \int_{S_B(t)} \left[\frac{\partial \varphi}{\partial t} + \frac{1}{2}\nabla\varphi \cdot \nabla\varphi + gZ\right]\mathbf{n}_+ ds \\
= & -\rho g\Big[\int_{S_B^W(t)} Z\mathbf{n}_+ ds + \int_{S_I^W(t)} Z\mathbf{n}_- ds\Big] \\
& -\rho\frac{d}{dt}\Big[\int_{S_B^W(t)} \varphi_I\mathbf{n}_+ ds + \int_{S_I^W(t)} \varphi_I\mathbf{n}_- ds\Big] \\
& -\rho\frac{d}{dt}\Big[\int_{S_B^W(t)} \varphi_D\mathbf{n}_+ ds\Big] \\
& -\rho\frac{d}{dt}\Big[\int_{S_T(t)+\Delta S(t)} \varphi_D\mathbf{n}_+ ds + \int_{S_I^E(t)} \varphi_D\mathbf{n}_- ds\Big] + \rho\frac{d}{dt}\Big[\int_{S_I^E(t)} \varphi_D\mathbf{n}_- ds\Big] \\
& -\rho\frac{d}{dt}\Big[\int_{S_T(t)+\Delta S(t)} \varphi_I\mathbf{n}_+ ds + \int_{S_I^E(t)} \varphi_I\mathbf{n}_- ds\Big] \\
& -\rho g\Big[\int_{S_T(t)+\Delta S(t)} Z\mathbf{n}_+ ds + \int_{S_I^E(t)} Z\mathbf{n}_- ds\Big]
\end{aligned}
\tag{3.19}
$$

3.2.1 Nonlinear buoyancy force

The first term on the RHS of Equation 3.19 represents the nonlinear buoyancy force. Applying Gauss' theorem:

$$
\mathbf{F}_{B,1}(t) = -\rho g\Big[\int_{S_B^W(t)} Z\mathbf{n}_+ ds + \int_{S_I^W(t)} Z\mathbf{n}_- ds\Big] = \rho g \forall_W(t)\mathbf{k}
\tag{3.20}
$$

Herein, $\forall_W(t)$ is the volume enclosed by the body wetted surface and the ambient wave surface interior to the body and $\mathbf{k}$ is the unit vector pointing in the positive z-direction. From the equation is possible to notice that the nonlinear hydrostatic force on the floating body point vertically upwards.

3.2.2 Froude-Krylov impulse force

The second term on the RHS of Equation 3.19 represents the nonlinear Froude-Krylov force which is defined as the time derivative of the Froude-Krylov impulse.

$$\mathbf{F}_{B,2}(t) = -\rho \frac{d}{dt} \Big[\int_{S_B^W(t)} \varphi_I \mathbf{n}_+ ds + \int_{S_I^W(t)} \varphi_I \mathbf{n}_- ds \Big] = \frac{d\mathbf{I}_{F-K}}{dt} \qquad (3.21)$$

$$\mathbf{I}_{F-K} = -\rho \int_{S_B^W(t)} \varphi_I \mathbf{n}_+ ds - \rho \int_{S_I^W(t)} \varphi_I \mathbf{n}_- ds = \rho \int \int_{\forall_W(t)} \nabla \varphi_I dv \qquad (3.22)$$

Where $\mathbf{I}_{F-K}$ is defined as FK impulse.

3.2.3 Radiation and diffraction body and free surface impulses and forces

The third term on the RHS of Equation 3.19 represents the body radiation and diffraction disturbance impulse and force, while the fourth and fifth terms are the radiation and diffraction disturbance over the ambient wave free surface. This terms has not been taken into account. The free surface radiation and diffraction impulse is small compared to the Froude-Krylov impulse and the body radiation and diffraction forces may be neglected.

3.2.4 Results obtained applying Sclavounos method

As done for the pressure integration method, also with Sclavounos approach, it has been evaluated the buoyancy and Froude-Krylow force considering the body at his mean position. The results are presented in Figure 3.8. From the figure it can be clearly seen that in this case the Froude-Krylov force has a smoother shape compared to the one obtained using the pressure integration method. Furthermore, also the magnitude of this force is smaller.
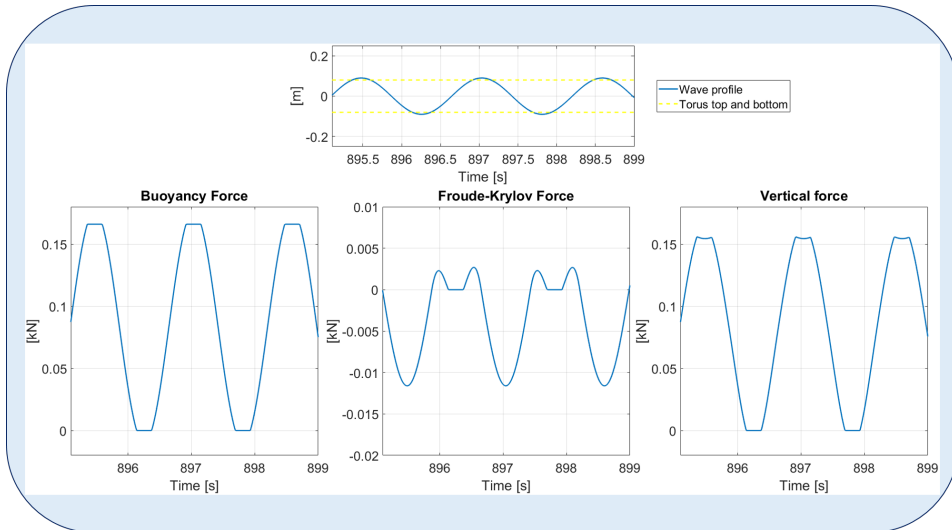
Figure 3.8: Linear buoyancy and Froude-Krylov forces acting on the torus for the case with H=9 m and T=11 s calculated applying Sclavounos method.

To calculate the strongly nonlinear buoyancy and Froude-Krylov forces the time dependent position of the torus and the time dependent wave elevation have been taken into account. Considering the shallow-water approximation the body wetted surface, necessary to calculate both buoyancy and Froude-Krylov forces, have been always computed as the difference between the bottom of the torus and the wave elevation at each time instant, which means that the force in considered to be constant along the x-direction at each time step.
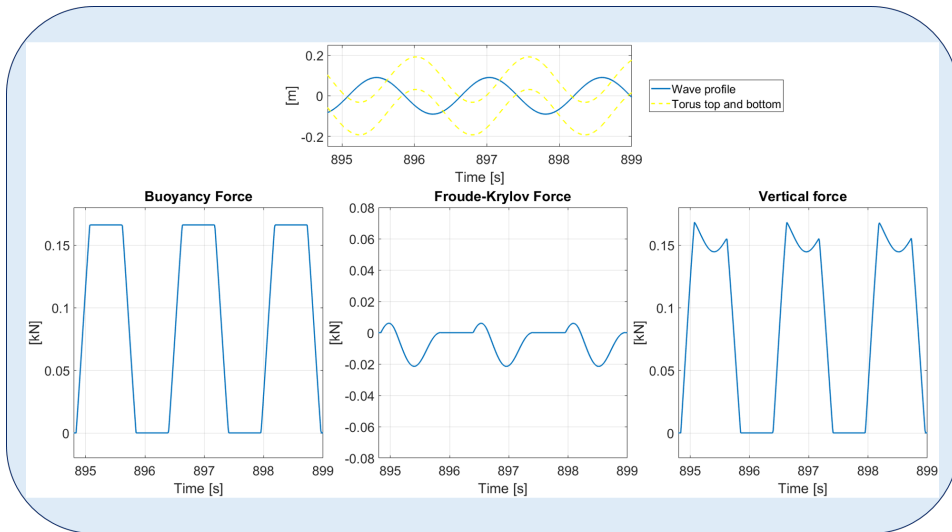
Figure 3.9: Nonlinear buoyancy and Froude-Krylov forces acting on the torus for the case with H=9 m and T=11 s calculated applying Sclavounos method.

Figure 3.11 shows that considering the Froude-Krylov force it has been noticed that evaluating the velocity of the body constant in the vertical direction and multiplying it for the wetted surface of the torus gives results close to the formulation presented where is considered the difference of the velocities, plotted in Figure 3.10.
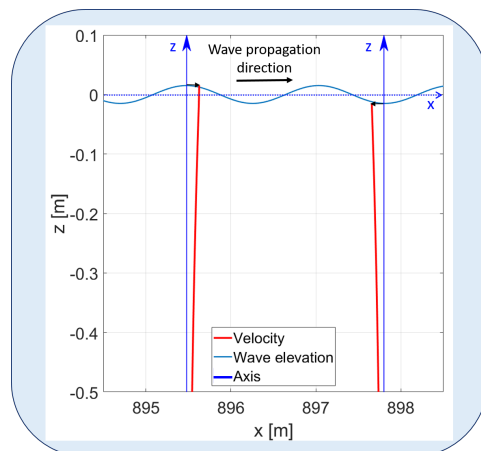
Figure 3.10: Horizontal velocity distribution under a wave crest and under a wave trough according to the linear theory.
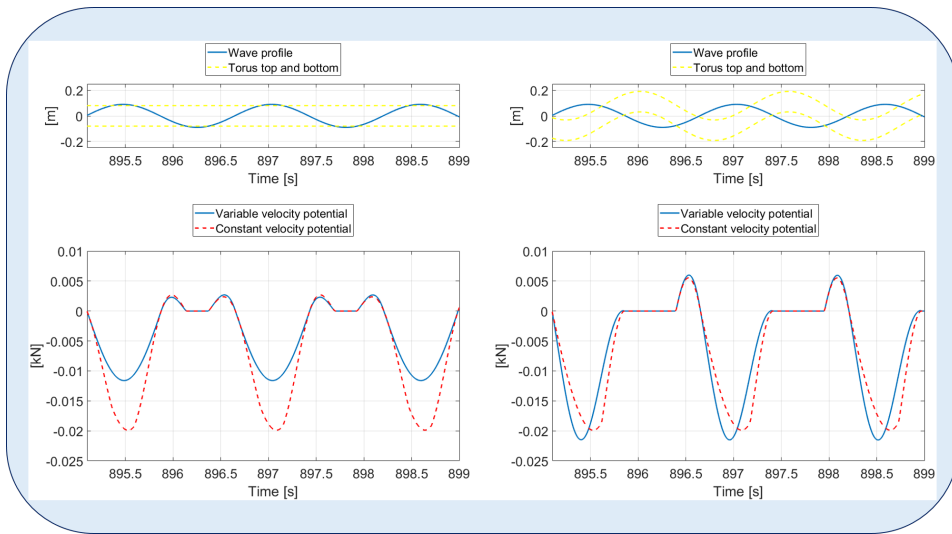
Figure 3.11: Difference in considering constant or varying velocity in Sclavounos method.

3.3 Comparison between the pressure integration method and Sclavounos method

Finally, in Figure 3.12 and in Figure 3.13 are presented the comparison between the two methods considered for calculating the buoyancy and Froude-Krylov forces.
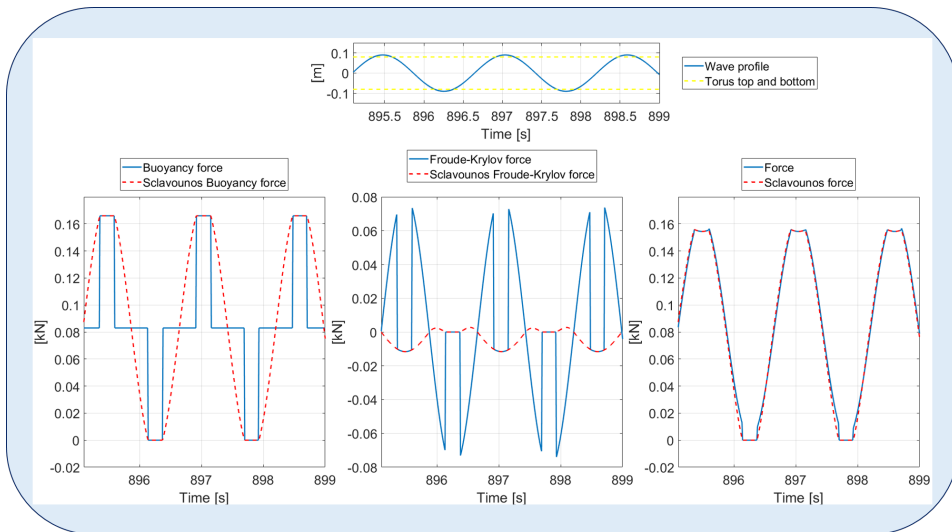
Figure 3.12: Comparison between the pressure integration and Sclavounos method for the case with H=9 m and T=11 s and the structure at mean water level.

For both the case with torus at mean water level and with the torus moving, it can be clearly seen that both the buoyancy and Froude-Krylov forces present a different behaviour. If the sum of the vertical force is considered, it can be notice that the results are really close. For the case with the floater at mean water level the vertical force is almost the same while for the case that consider the motion of the torus, a small difference is noted for the time in which the body is fully submerged.
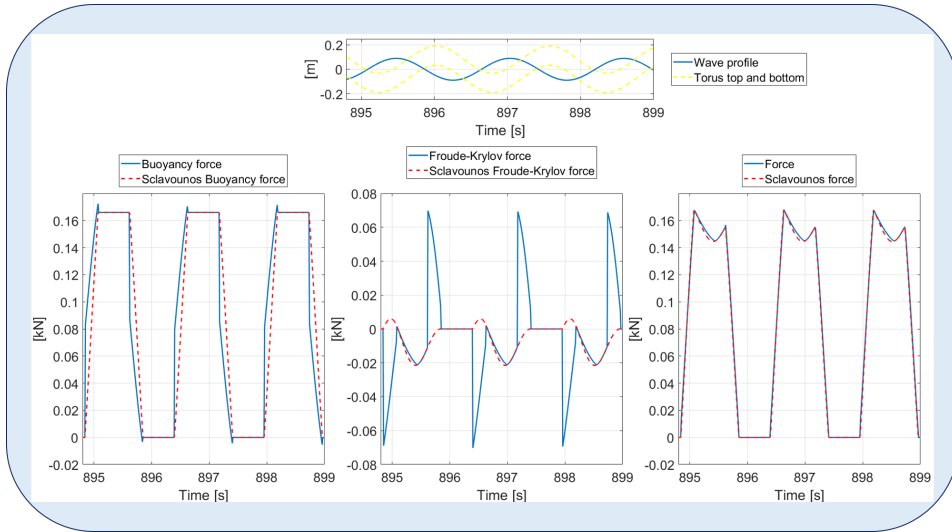
Figure 3.13: Comparison between the pressure integration and Sclavounos method for the case with H=9 m and T=11 s considering the motion of the structure.

As Sclavounos method presents an easier formulation it has been chosen as solution to be implemented in SIMO.

4 | Chapter

Experimental results

4.1 Description of the model test

In order to have a clear understanding of the test results is important to understand the conditions under which the model tests have been carried out. For this reason this section describes the test set up. The information have been taken from the doctoral thesis of Ling Wan [2].
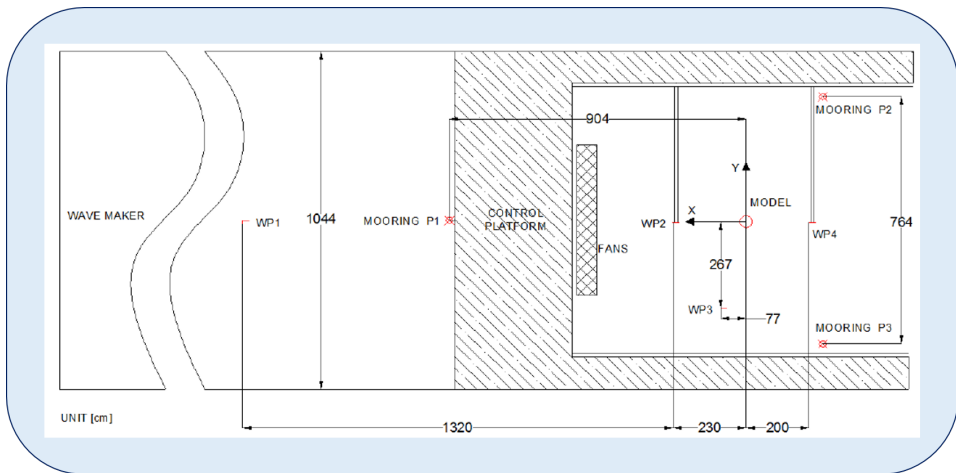
Figure 4.1: Layout for the testing facility in the MAARINTEK [2].

The test set up layout in the MARINTEK towing tank is shown in figure 4.1. The towing tank has a length of 260 m a breadth of 10.5 m and a water depth of 10/5.6 m. In the studied case the model was placed in the area with 10 m depth. During the tests four-resistance-type wave probes were used to evaluate the wave elevation, while the body motions have been tracked by cameras that were sending the data to the amplifiers and then to the control

system. The wind conditions have been generated by two rows of fans located in front of the model.

In the survivability test, eighteen HBM DF-2S water-proof bending load cells have been installed in order to measure the forces between the spar and the torus. The cells rigidly connected the bodies and measured the total forces. The body motions have been recorded using the Qualis system with 3 reflection balls and 8 cameras.

4.2 Model used for the MARINTEK survivability test
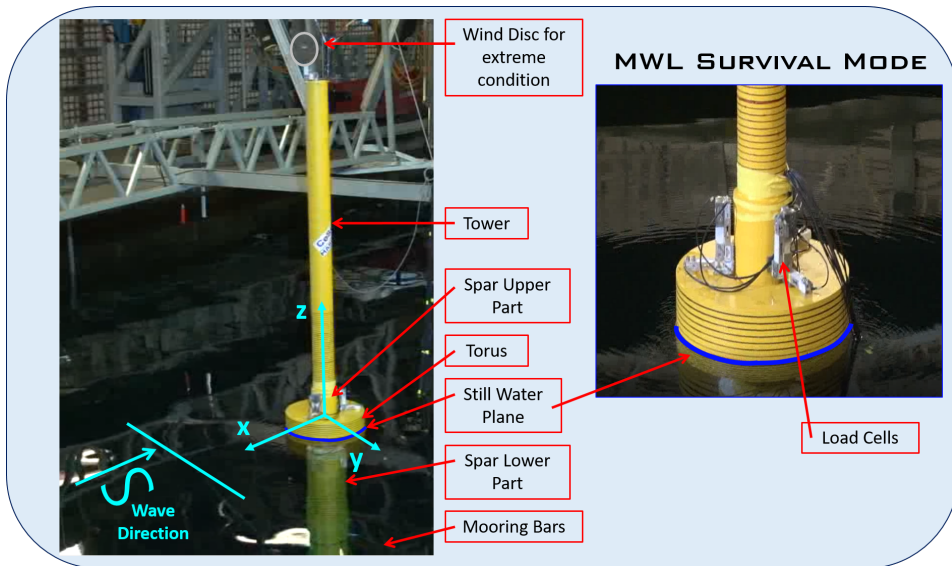
Figure 4.2: STC model, coordinate systems and various components in the MWL with large disc survival modes in the MARINTEK survivability test.

In Figure 4.2 is presented physical model that have been used in the MARINTEK survivability test. Figure 4.2 shows the inertial coordinate system used, where the z-direction is positive upwards, x-direction is positive in the wave maker direction and the y-direction is established following the right-hand rule. The origin is set at the intersection between the still water surface and the vertical axis of the spar.

In the survivability tests, the aerodynamic effect of the wind turbine have been modelled using a small disk with a diameter of 15 cm, while in the operational conditions the disk diameter used if of 1.85 m.

The dimension at full scale of the model tested at MARINTEK are presented in Table 4.1, while in Table 4.2 the mass properties for the MWL model are reported.

Finally in Table 4.3 shows the natural period and the damping ratios, already presented in Table 1.4, founded performing the decay tests are presented for surge, sway, heave, roll and pitch.

	Dimension	
Spar lower portion	Diameter [m]	10
	Length [m]	108
Spar upper portion	Diameter [m]	6.45
	Length [m]	24
Tower	Diameter [m]	5.5
	Length [m]	77
Spar and Tower	Draft for MWL mode [m]	122
Torus	Height [m]	8
	Outer diameter [m]	20
	Inner diameter [m]	8
	Draft for MWL mode [m]	4

Table 4.1: Dimensions of the models tested at MARINTEK at full scale [2].

Mass properties MWL survival mode		STC	Spar, Tower and Wind Turbine	Torus
Total weight [ton]		10036.25	8891.25	1145.00
Ballast [ton]		4276.25	4276.25	0.00
C.O.G. form WL [m]		67.50	76.50	0.00
Radius of gyration	R_{xx}	88.50	94.50	7.00
	R_{yy}	88.50	94.50	7.00
with respect to WL [m]	R_{zz}	4.5	4.00	7.00

Table 4.2: Mass properties in the MWL survivability mode for the model tested at MARINTEK [2].

D.O.F.	**Surge**	**Sway**	**Heave**	**Roll**	**Pitch**
Natural periods [s]	98	93.1	12.8	36	36.6
Damping ratios [%]	4.4	-	6.5	-	4

Table 4.3: Natural periods and damping ratios for the MWL survival mode [2].

Finally in Table 4.4 are presented the scaling factors for different variables. The model tested at MARINTEK was down scaled using Froude scaling with a ratio of 1:50.

Variables	**Scale factor**	**Value**
Linear Dimensions (D)	λ	1:50
Fluid or structure velocity (u)	$\lambda^{1/2}$	1:7.07
Fluid or structure acceleration (a)	1	1:1
Time or period (t)	$\lambda^{1/2}$	1:7.07
Structure mass (m)	λ^3	$1:1.25\cdot10^5$
Structure displacement volume (V)	λ^3	$1:1.25\cdot10^5$
Force (F)	λ^3	$1:1.25\cdot10^5$
Moment (M)	λ^4	$1:6.25\cdot10^6$

Table 4.4: Scaling factors for different variables [2].

4.3 Test results

In this section, some results for the three environmental conditions studied for the STC in the MWL survival mode are presented 4.5.

The test examined have been carried out with regular waves.

MWL STUDY CASES			
H [m]	9	9	9
T [s]	11	13	15

Table 4.5: Regular wave test studied in order to investigate the slamming phenomena.

Due to the shallow draft of the torus and the large body motions, in the survivability model test the phenomena of water entry and exit is accompanied by slamming and water on deck. The nonlinear phenomena have been observed for-incident wave periods within the resonance region of heave motion.

In Figure 4.3 presents the snapshots for the incident waves with H=9 m and T=13 s. From the figure it can be clearly seen that being the waves regular, slamming is periodic. Furthermore it can be notice that the magnitude of the vertical force is much bigger than the magnitude of horizontal force. As previously pointed out, it is possible to see how slamming loads appears in both the vertical and the horizontal forces.
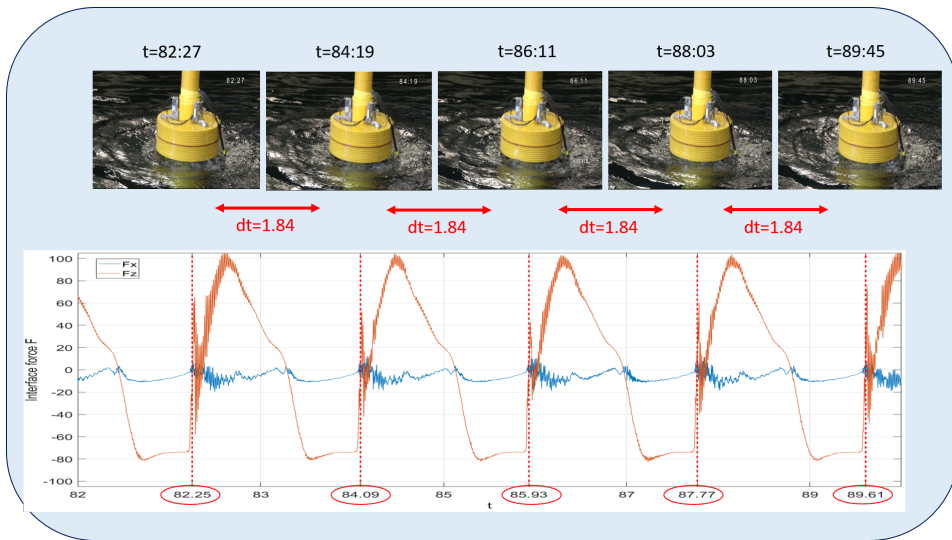
Figure 4.3: Strongly nonlinear phenomena in the model test for incident waves with H=9 m and T=13 s.

Figure 4.5 shows the physical investigation of motions and interface forces for the incident waves with H=9 m and T=13 s. In the lower part the relative vertical motion, heave and pitch motions are plotted. The relative vertical motion (s_r) is defined as the difference

between undisturbed wave elevation (ζ_0) estimated at the origin of the coordinate system and the measured heave motion of the torus (η_3):

$$s_r = \zeta_0 - \eta_3 \tag{4.1}$$

In order to define when the torus is totally in or out of the water the relative vertical motion and the torus draft and freeboard are compared assuming the wave length to be much bigger then the torus diameter and the surge motion at the still water line small compared with the wave length.

In the figure both x and y axes are non-dimensional, indeed the time is divided by the wave period T, the transnational motions are divided by the incident-wave amplitude $\zeta_a = H/2$, the rotational motions are divided by the incident wave steepness $k\zeta_a$, while the force parameters are divided by $\rho V g$ with ρ the density of the water, V the submerged volume of the torus and g the gravitational acceleration.

To better understand Figure 4.5, the different phenomena and the position of the STC can be seen in Figure 4.4 and described as:
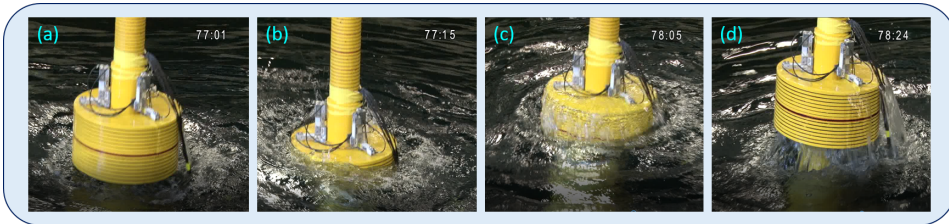
Figure 4.4: Strongly nonlinear phenomena in the model test for incident waves with H=9 m and T=13 s. In order from the left: water entry (a,b), green water (b,c) and water exit (c,d).
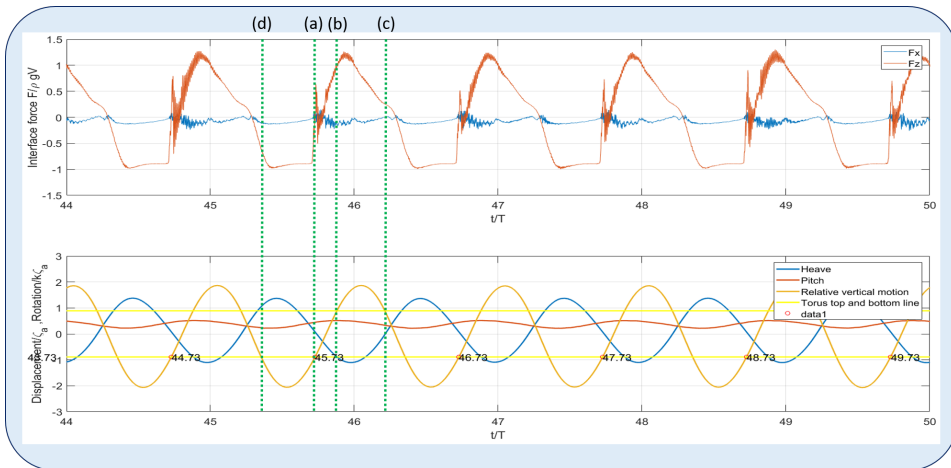
Figure 4.5: Physical investigation of motions and interface forces for the cases with H=9 and T=13.

a) water entry:

    beginning stage of the wave entry event. The torus is going downwards and the pitch motion is negative. This condition induces high-frequency and relevant peaks on the interface force;

b) water entry/green water:

    at this instant the water reaches the torus top and invades the deck, starting the WOD event;

c) green water/water exit:

    after have reached the maximum amount of water shipping the torus goes upwards and reach instant c where the torus starts going out of the water;

d) water exit:

   at this instant the torus is totally out of the water, the gravity force starts to be dominant. This instant is followed by a new water-entry event with slamming.

The occurrence of slamming and WOD is also plotted in Figure 4.6. In both Figure 4.5 and 4.6 the yellow lines represent the top and the bottom of the torus.

In the process described, characterized by the WEE, slamming and WOD phenomena, the interface forces are strongly influenced by the nonlinear forces induced by the incident waves while the motions responses are not significantly affected.

Finally it is important to notice how, in the test done for the MWL survival mode the heave motion amplitude is not the only parameter affecting the slamming peaks but also the relative phases between the different motions and the wave elevation counts.
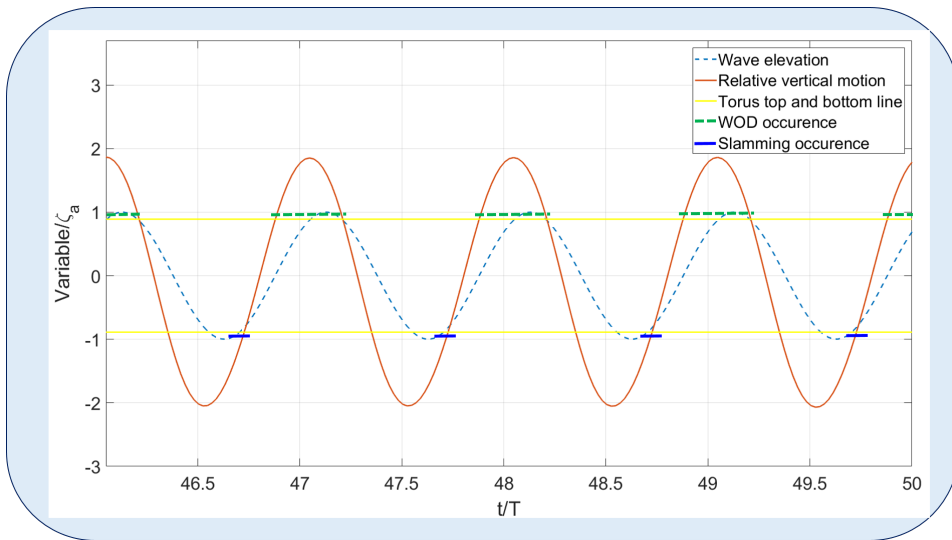
Figure 4.6: Occurrence of slamming and green water for the cases with H=9 and T=13.

4.4 Slamming peaks and validity of the slamming model selected

Table 4.6 shows the experimental results for the slamming force that are also plotted in Figure 4.7. As explained in the Slamming Chapter, in order to predict the slamming force is necessary to know the relative angle of the torus and the velocity at the impact instant. This data are reported in the table below together with the results obtained from the MATLAB script for the slamming force. As it can be clearly seen from the table the results are quite accurate. Furthermore it can be notice that the angle at the impact instant is between 4 and 5 degrees.

Slamming					
Time [s]	82.25	84.09	85.93	87.77	89.61
Relative angle [Deg]	4.814	4.830	4.834	4.845	4.859
Velocity at the impact instant [m/s]	0.325	0.323	0.320	0.320	0.325
Force peaks due to slamming					
Experimental results [N]	82.25	84.09	85.93	87.77	89.61
Calculated in MATLAB [N]	86.69	85.34	83.70	83.50	85.90

Table 4.6: Slamming force and parameters for the calculation of the slamming in MATLAB.
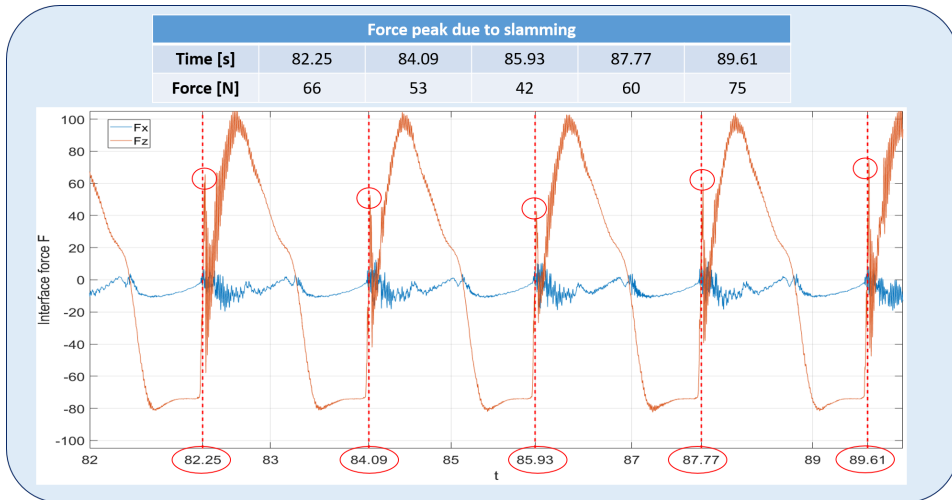
Figure 4.7: Slamming peaks for the cases with H=9 and T=13.

Chapter 5

Numerical analysis

5.1 Inroduction

In this Thesis, in order to study the behaviour of the STC in the MWL survival mode under extreme environmental conditions, numerical simulations are performed using the time-domain code SIMO [3] , which is based on the linear potential theory. Furthermore, a simplified nonlinear wave load model in SIMO (which is basically a correction of the linear model considering the nonlinear buoyancy force, the nonlinear Froude-Krylovforce, and the slamming force) have been developed and implemented in the code.

SIMO is a time domain simulation program for investigate the motions and station keeping of multibody systems. It includes flexible modelling of station keeping forces and connecting force mechanisms.

SIMO calculates the response by nonlinear time domain analysis by imposing dynamic equilibrium in every time step. As explained in the introduction section, the dynamic equation of motion depends on both time and frequency. Retardation functions consider the frequency dependent added mass, damping terms and harmonic loading [44]. The frequency domain equation of motion is reached starting from the dynamic equation of motion in time domain and then applying a convolution theorem, Fourier transform and establishing the retardation functions. The aim of retardation functions is to calculate simultaneous response dependent on both frequency and time.

The works done by the external loads is equal to the works absorbed by the structure which includes internal, dissipative and inertial forces and is used to account the structural damping. The main assumption of Rayleigh damping is that the damping is proportional to the mass and stiffness matrices of the dynamic equation of motion.

The Newmark-Beta implicit iteration method is used for time integration.

In case of load histories with turning points and limit points, the load-displacement history is calculated applying Newton-Raphson method.

As SIMO is a linear code, it calculates linear buoyancy and Froude-Krylov forces.

5.1.1 Simulation parameters

In Table 5.1 are listed the time parameters of the simulations. Time step identify the time length at which the dynamic equilibrium equation is solved by SIMO, while the time increment is the time in which SIMO records the outputs requested.

Simulation Length	Time step	Requested time series length	Time increment
5000 s	0.001 s	5000 s	0.005

Table 5.1: SIMO simulation's parameter.

5.2 Nonlinear numerical modelling

To obtain accurate results in SIMO slamming, nonlinear buoyancy and nonlinear Froude-Krylov forces are studied and implemented to the solver. If for the slamming analysis the angle between the torus and the local slope of the incident waves in the incident-wave direction is considered, both the nonlinear buoyancy and the nonlinear Froude-Krylov are estimated considering the shallow-water approximation, being the waves long in the studied cases.

The impact on the bottom of torus is considered to start from the outer circle, being the incident waves sufficiently long. The evaluation of the angle between the torus and the incident wave make possible to apply a strip-theory approach in the local x-direction. For each strip the local Wagner-type solution.

This force components are then added to the equation of motion at each time step to describe the dynamic responses of the STC.

5.2.1 Slamming

As pointed out in the Slamming chapter, the slamming loads are founded considering:

- instant of the impact (t_i)

- velocity at the instant of the impact V_0

- angle at the instant of the impact β

The solution have been chosen after the analysis of the experimental results where the impact angle has been founded to be in the order of $2°$ - $5°$. The angle depends mostly on the pitch angle of the structure, being the waves considered long. As it can be clearly seen in Figure 5.1 the pitch in the simulation done with SIMO is not stable and does not converge. Furthermore the pitch angle, shown in Figure 5.2 has been founded to be with a value always close to zero at the instant of the impact. This mean that the slamming solution proposed, based on the velocity and the angle of the experiments, is not reliable. Indeed with small angles the method analyzed gives really high value which does not allow SIMO to find the equilibrium at each time step.

An unstable behaviour, as shown in Appendix A have been founded also for the surge,

sway and roll motions. Furthermore heave and yaw motions are convergent but presents an offset.
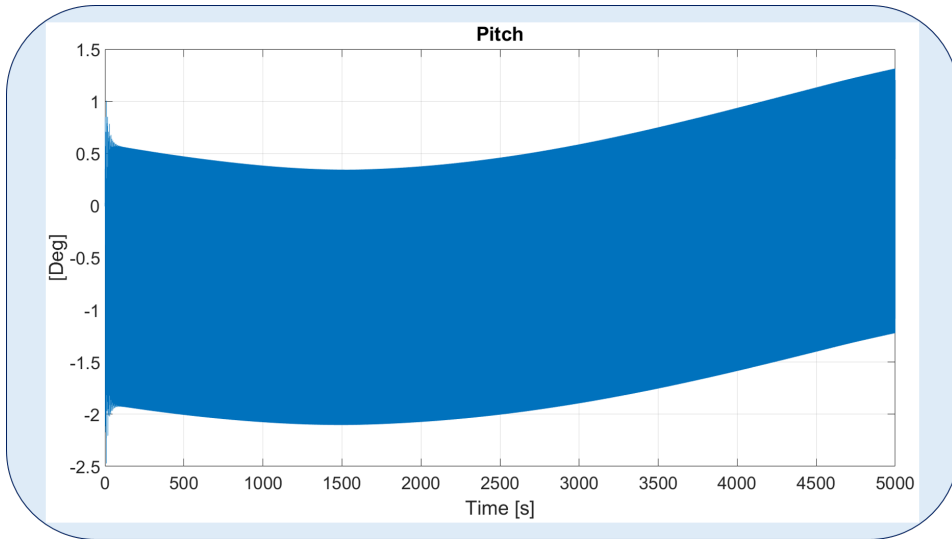
Figure 5.1: Pitch angle for the case with H=9 m and T=11 s.
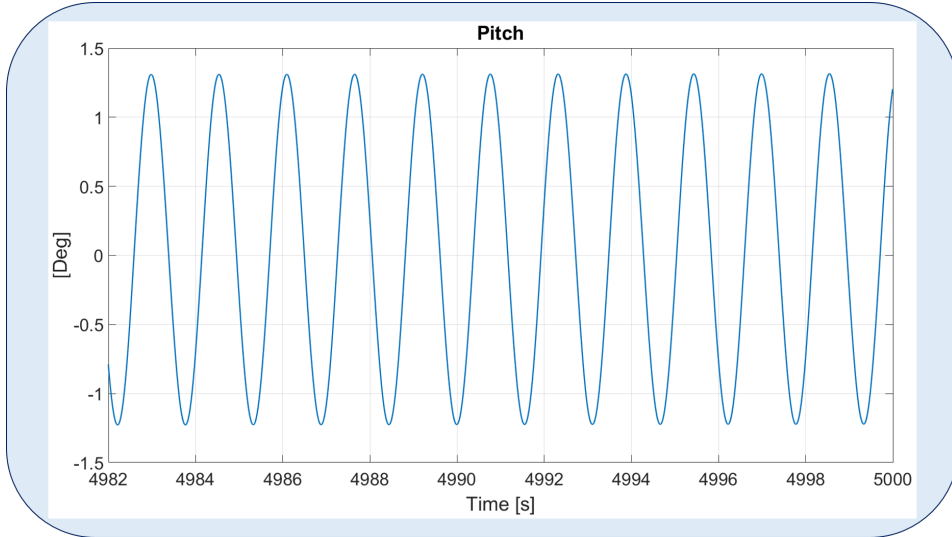
Figure 5.2: Focus on the pitch angle for for the case with H=9 m and T=11 s.

The unstable behaviour of the pitch could be caused by the nonlinear Buoyancy and Froude-Krylov forces that are applied to the center of the torus in the z-vertical direction. This loads could cause a moment that makes the simulation unstable. But what is

clear, also when no external forces are added is that the pitch of the model does not agree with the experimental data. This means that is not possible to implement the external DLL slamming force to the torus.

### 5.2.2 Nonlinear buoyancy and Froude-Krylov forces

As explained in the chapter Nonlinear buoyancy and nonlinear Froude-Krylov forces, Sclavounos method has been chosen to evaluate the nonlinear buoyancy and nonlinear Froude-Krylov loads on the STC.
As the linear forces are already considered by SIMO it have been necessary to remove from the total nonlinear vertical force calculated with Sclavounos method the linear part. Considering the equation of motion in the vertical direction:

$$(M_{33} + A_{33})\ddot{x}_3(t) + B_{33}\dot{x}_3(t) + C_{33}x_3(t) = F'_D(t) + F'_{FK}(t) \tag{5.1}$$

and defining F_V as the sum of nonlinear buoyancy and nonlinear Froude-Krylov:

$$(M_{33} + A_{33})\ddot{x}_3(t) + B_{33}\dot{x}_3(t) = F_V(t) - (F'_{FK}(t) - C_{33}x_3(t)) + F'_D(t) \tag{5.2}$$
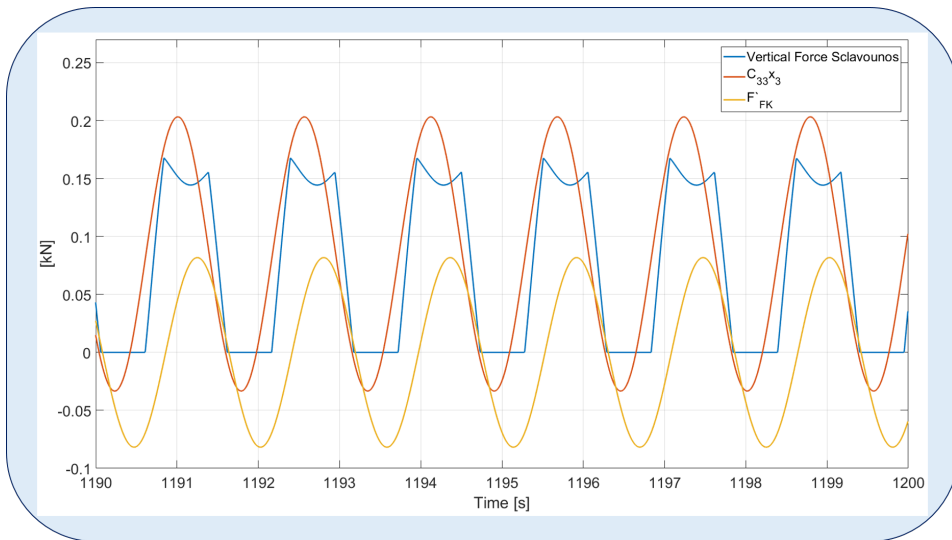
Figure 5.3: Vertical nonlinear Sclavounos, linear hydrostatic and linear Froude-Krylov forces for the case with H=9 m and T=11 s.

Figure 5.3 shows the vertical nonlinear Sclavounos, linear hydrostatic and linear Froude-Krylov forces while in Figure 5.4 is presented the total nonlinear load that have been implemented as external DLL force and implemented in the SIMO analysis.
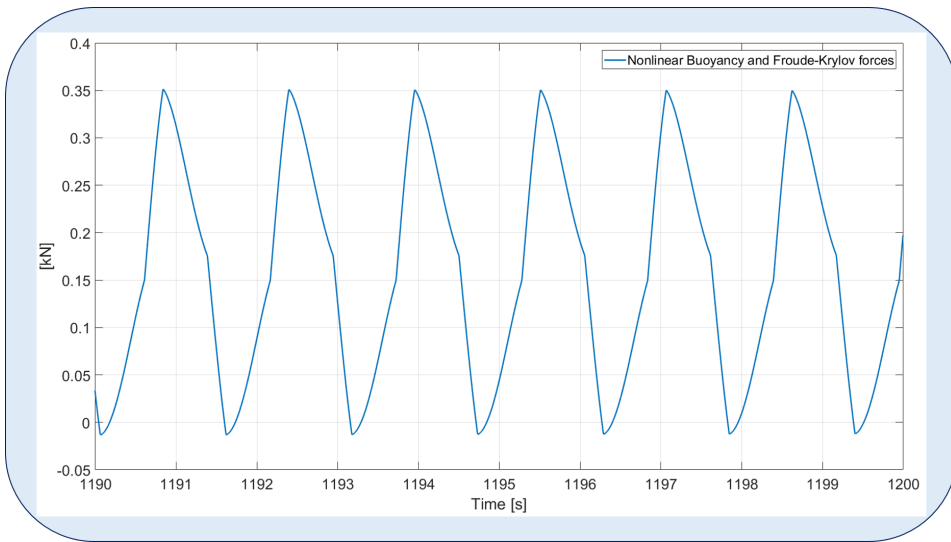
Figure 5.4: Total nonlinear load for the case with H=9 m and T=11 s.
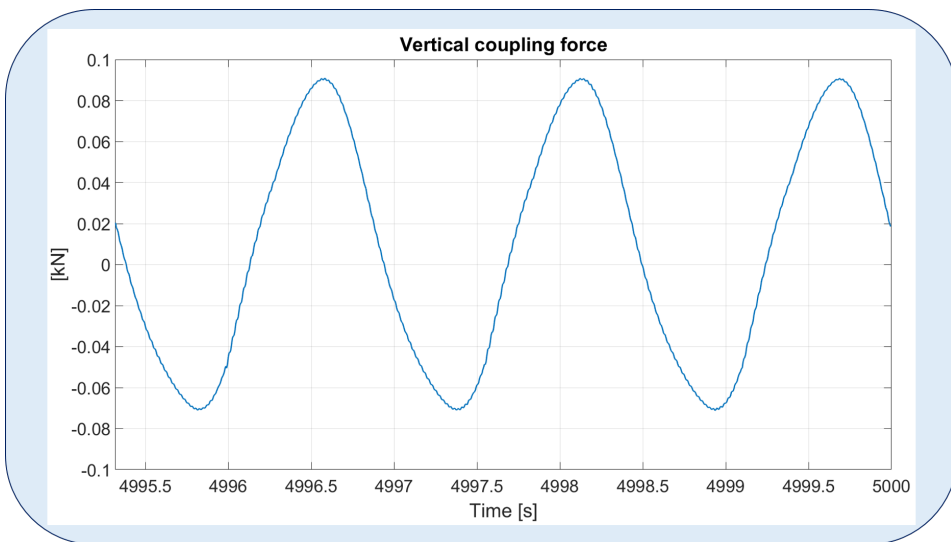
5.3 MWL SIMO tests

5.3.1 H=9 m and T=11 s

Figure 5.5: Coupling force in the vertical direction for the case with H=9 m and T=11 s.

Figure 5.5 presents the results of the interface force in the z-vertical direction for the case with H=9 m and T=11 s. As explained before, this is the numerical results obtained from the SIMO simulation in which the nonlinear buoyancy and nonlinear Froude-krylov forces calculated using Sclavounos method have been implemented to the model as external force. In the figure it can be notice that the vertical force increases while the body is going into the water and reach the minimum value when the body is completely out of water. The force is periodic being the test done in regular wave conditions.

5.3.2 MWL test for H=9 m and T=23 s (linear case)

Figure 5.6 presents the numerical results of the analysis of the linear case (H=9 m and T=23) of the STC in the MWL survival mode. The motions of this simulation, presented in appendix A, are all convergent. In this case there is not the necessity to implement additional loads to the analysis. From the figure it can be seen that the forces on the structure are much smaller. Indeed in this case the structure is never fully submerged or out of water so the loads results to be reduced compared to the one presented in Figure 5.5.
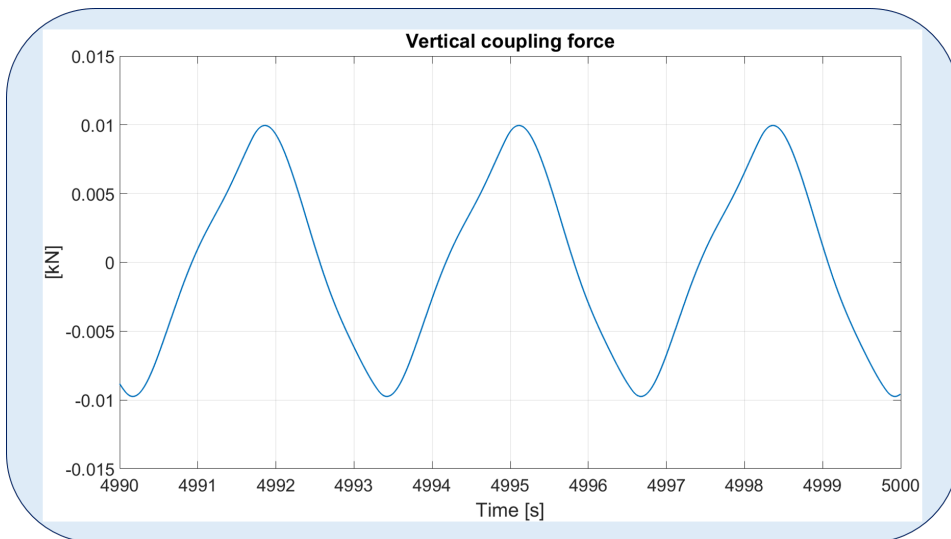
Figure 5.6: Coupling force in the vertical direction for the case with H=9 m and T=23 s.

5.4 Comparison of experimental and numerical results

5.4.1 MWL test for H=9 m and T=11 s

Figure 5.7 presents both the experimental and the numerical results of the interface force in the z-vertical direction for the case with H=9 m and T=11 s. The different phase, explained in Figure 4.5 can be founded in both the experimental and numerical results. From the figure it can clearly seen the accuracy of the maximum value of the force while

the behaviour of the body when body out of water is not accurate. indeed this phase seems to last much longer in the experimental results. Furthermore the curve of the experimental results shows the slamming loads and the vibrations that are consequence of the violent impact of the structure. For the numerical results, as explained this force have not been implemented.
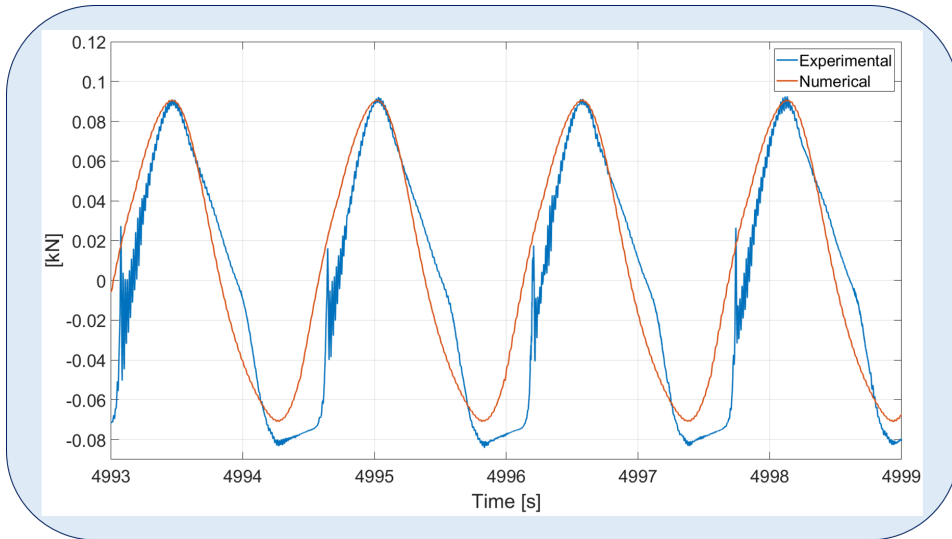
Figure 5.7: Comparison of numerical and experimental results for the coupling force in the vertical direction for the case with H=9 m and T=11 s.

Conclusion discussion and recommendations for Future Work

6.1 Conclusion

When the STC have been tested adopting MWL survival mode under extreme sea states, the resonance in heave was excited. This induces large heave motions and wave impacts on the torus. Due to the resonant behaviors and the strongly nonlinear phenomena the linear model in SIMO can not provide reliable results. This is why in this Thesis the nonlinear loads have been investigated.
In order to understand motions and loads of the STC in the MWL survival mode, the equation of motion have been presented together with a detailed analysis on slamming, nonlinear buoyancy and nonlinear Froude-Krylov forces.

Slamming has been defined as an impulse loads with high pressure peaks that occurs during the impact between the torus and the water. It has been pointed out how the duration of slamming pressure is of the order of milliseconds and it is very localized in space. Furthermore, the position where high slamming pressure occurs changes with time and depends on how the water hits the structure.
The shallow draft of the torus and the large body motions in the survivability model test caused the phenomena of water entry and exit is accompanied by slamming and water on deck that have been explained. The nonlinear phenomena have been observed for incident wave periods within the resonance region of heave motion. But as explained the slamming peaks are not affected only by the heave motion amplitude but also by the relative phases between the different motions and the wave elevation.
The strip theory approach in the local x direction have been chosen to study the problem. In each strip the local Wagner-type solution for the bottom slamming is applied. This theory assumes that the free surface can be approximated to a straight line at the impact location, that the spatial and time scales are so small that the local solution is studied as a

perturbation of the flow variables numerically at the impact instant and that no air cavities are formed on the front side.

The linear wave theory has been used in order to determine the nonlinear buoyancy and nonlinear Froude-Krylov forces on the STC. Nonlinear forces are caused by the heave motion of the torus which on the analyzed conditions passes from being totally submerged to be completely out of the water. Nonlinear buoyancy and nonlinear Froude-krylov forces have been investigated with both the pressure integration and Sclavounos methods. The pressure integration method consist on the integration over the wetted surface of the hydrostatic and dynamic pressure. The behaviour of the nonlinear Froude-Krylov force resulted to be strange so in order to confirm the accuracy of the results it has been compared with the results given by Sclavounos method.

Sclavounos method has been developed in order to save computational time while studying the nonlinear loads exerted on a floating body by steep irregular surface waves. Forces and moments are calculated deriving in time the fluid impulse, while in the traditional approach the terms of Bernoulli's equation are derived in time and space. The application of this method leads to the generalized equations of motions for a rigid body in an ideal fluid. According to this method, the nonlinear wave force acting on the body is the sum of the nonlinear hydrostatic force to the time derivative of the Froude-Krylov and radiation-diffraction impulses. The nonlinear hydrostatic force on the floating body is shown to point vertically upwards and the nonlinear Froude-Krylovforce is defined as the time derivative of the Froude-Krylov impulse. Nonlinear radiation and diffraction forces are expressed as time derivative of two impulse, a free surface impulse and a body impulse but they haven't been considered in this work.

The comparison of the results provided from the two method for both the case in which the torus is at mean water level and for the case in which is considered the motion of the structure confirmed the accuracy of the calculations.

Once the nonlinear loads have been studied and the results for the STC plotted using MATLAB, the numerical analysis using the linear time domain code SIMO started. The MATLAB codes have been translated into Fortran in order to create a DLL which is then implemented in SIMO as external force at each time step of the simulation. The results of the nonlinear buoyancy and nonlinear Froude-Krylov forces resulted to be consistent with the experimental results. The implementation of slamming loads showed that something in the simulation went wrong. The motions of the structure resulted to not be convergent and the relative angle between the bottom of the torus and the free-surface resulted to be much smaller than the one obtained from the experiments in the MARINTEK's towing tank. This instability of the motions could be caused by the implementation of nonlinear buoyancy and Froude-Krylov forces, while the reduced pitch angle could be caused by some problems in the model used for the SIMO simulations.

6.2   Discussion

The study of the hydrodynamic loads acting on the STC have been really interesting and challenging. Finally, once the results for slamming, nonlinear buoyancy and Froude-Krylov forces have been founded with great disappointment it comes out the problem of the relative angle of the torus that blocked the implementation of the slamming force.

All the studies related to this topic gave me a deeper knowledge on hydrodynamic loads on a floating structure. With more time it would have been interesting to see from a structural point of view the influence of this forces on the torus bottom and to analyze the vibrations induced by the slamming loads on the structure in extreme extreme environmental conditions that could compromise the structural integrity.

6.3   Future work

The aim of this Thesis was to understand the model, the slamming phenomena and the nonlinear buoyancy and Froude-Krylov forces. Based on this work recommendations for future work can be summarized as follows:

- Detailed study of the body motion in the SIMO simulations and analysis on the pitch angle of the structure. Also without the addition of the nonlinear loads, the pitch angle results to be much smaller than the one measured in the experimental test. A check on the model could lead to the correction of this problem.

- Implementation in SIMO of the proposed slamming model. The slamming model proposed gives good results considering the velocity and the angle at the impact instant of the experimental results. Once the problem of convergence and motions are fixed in SIMO the implementation of the slamming loads could give really accurate results and the comparison with the experimental results could be really close.

- Structural analysis considering the slamming loads. Implementing the slamming force and reaching consistent results could be the starting point to study the effects of the loads on the STC in the MWL survival mode. The analysis should include the effect caused by the vibration that are created by the impact of the structure with the free surface.

Bibliography

[1] *https://cordis.europa.eu/project/rcn/93425_en.html*, visited last April 2018.

[2] Wan, L., *Experimental and Numerical Study of a Combined Offshore Wind and Wave Energy Converter Concept*, Department of Marine Technology Norwegian University of Science and Technology (NTNU), Thesis for degree of Philosophiae Doctor, Trondheim, June 2016.

[3] SIMO project team, *SIMO theory manual Version 4.0 rev.0*, MARINTEK, 2012.

[4] *IPCC Fifth Assessment Report, 2014*
United States Global Change Research Program, "Global Climate Change Impacts in the United States," Cambridge University Press, 2009
Naomi Oreskes, "The Scientific Consensus on Climate Change," Science 3 December 2004: Vol. 306 no. 5702 p. 1686 DOI: 10.1126/science.1103618

[5] National Research Council (NRC), *Surface Temperature Reconstructions For the Last 2,000 Years*, National Academy Press, Washington, D.C, 2006.

[6] *https://climate.nasa.gov*, visited last April 2018.

[7] *http://wwf.panda.org/about_our_earth/species/problems/climate_change/*, visited last April 2018.

[8] United States Department of Energy, *https://www.netl.doe.gov/research/coal/carbon-storage/carbon-storage-faqs/what-are-the-primary-sources-of-co2*, visited last April 2018.

[9] *https://en.wikipedia.org/wiki/Wind_power*, visited last April 2018.

[10] Kaldellis, J. K., Zafirakis, D., *The wind energy (r)evolution: A short review of a long history*, Renewable Energy, Volume 36, Issue 7, July 2011, Pages 1887-1901.

[11] Bachynski, E. E., Gao, Z., *Introduction to offshore wind power and technology*, Department of Marine Technology Norwegian University of Science and Technology (NTNU), Lecture 1, 2017.

[12] REN21, *Renewables 2016, Global status report* (Paris: REN21 Secretariat)

[13] Roddier, D., Cermelli, C., Weinstein, A., 2009. *WindFloat: A Floating Foundation for Offshore Wind TurbinesPart I: Design Basis and Qualification Process, Proceedings of the 28th International Conference on Ocean, Offshore and Arctic Engineering*, May 31 - June 5, Honolulu, USA, pp. 845-853.

[14] *https://www.statoil.com/en/what-we-do/hywind-where-the-wind-takes-us.html*, visited last April 2018.

[15] Butterfield, C. P., Musial, W., Jonkman, J., Sclavounos, P., Wayman, L., *Engineering challenges for floating offshore wind turbines*, National Renewable Energy Laboratory, 2007.

[16] Wenfei, X., Gao Z., *Design, numerical modelling and analysis of a spar floater supporting the DTU 10MW wind turbine*, Norwegian University of Science and Technology, June 2016.

[17] Alcorn, R., *Future Energy (Second Edition)*, Chapter 17 Wave Energy, Improved, Sustainable and Clean Options for our Planet 2014, Pages 357382.

[18] Cruz, J., *Ocean wave energy*, Springer Series in Green Energy and Technology, UK, 2008.

[19] Falnes, J., *Marine Structures*, A review of wave-energy extraction, Marine Structures Volume 20, Issue 4, October 2007, Pages 185-201.

[20] De O.Falcão, A. F., *Renewable and Sustainable Energy Reviews*, Wave energy utilization: A review of the technologies, Volume 14, Issue 3, April 2010, Pages 899-918.

[21] Falnes, J., *Ocean Waves and Oscillating Systems*,Linear Interactions Including Wave-Energy Extraction, Chapter 6, Cambridge University Press, 2002.

[22] Mouwen, F., *"Presentation to Engineers Ireland 2008"* (PDF), Engineers Ireland.

[23] Weber, J., Mouwen, F., Parrish, A., Robertson, D., *Wavebobresearch & development network and tools in the context of systems engineering*, Proceedings of 8th European Wave Tidal Energy Conference, Uppsala, Sweden (2009), pp. 416-420.

[24] WaveBob, *https://en.wikipedia.org/wiki/Wavebob*, visited last April 2018.

[25] ISSC Committee, *V.4 Offshore Renewable Energy*,The 19th International Ship and Offshore Structures Congress (ISSC) Report, 2015.

[26] Jonkman, J., Butterfield, S., Musial, W., Scott, G., *Definition of a 5-MW Reference Wind Turbine for Offshore System Development*, Technical Report/TP-500-38060, National Renewable Energy Laboratory, 2009.

[27] Li, L., Gao, Z., Moan, T., *Joint environmental data at five european offshore sites for design of combined wind and wave energy devices, Proceedings of the 32nd International Conference on Ocean, Offshore and Arctic Engineering*, June 9-14, Nantes,France, 2013.

[28] Greco, M., Lugni, C., *3-D seakeeping analysis with water on deck and slamming. Part 1: numerical solver*, Journal of fluids and structures, 33, 127-147, 2012.

[29] Greco, M., Bouscasse, B., Lugni, C., *3-D seakeeping analysis with water on deck and slamming. Part 2: Experiments and physical investigation*, Journal of fluids and structures, 33, 148-179, 2012.

[30] Muliawan, M. J., *Design and Analysis of Combined Floating Wave and Wind Power Facilities*, Thesis for degree of Philosophiae Doctor, Trondheim, June 2014.

[31] Kistnen, S., Gao Z., *Mathieu Instability of the Pitch Motion of the STC Concept*, Norwegian University of Science and Technology, December 2016.

[32] Liu, H., Gao Z., *Stress analysis of the structural interface between the spar and the torus in the combined wind and wave energy concept STC*, Norwegian University of Science and Technology, June 2016.

[33] DNV GL, *Environmental conditions and environmental loads*, DNVGL-RP-C205, DNV GL AS August 2017.

[34] Faltinsen, O. M., Landrini, M., Greco, M., *Slamming in marine applications*, Journal of Engineering Mathematics 48: 187217, 2004, Kluwer Academic Publishers.

[35] Faltinsen, O. M., *Sea loads on ship and offshore structures*, Professor, Department of Marine Technology Norwegian Institute of Technology, Cambridge University Press, 1990.

[36] Abramson, H. N., Bass, R. L., Faltinsen, O. M. Olsen, H. A., *Liquid Slosh in LNG Carriers*, In Proc. Tenth Symp. on Naval Hydrodynamics, ed. R. D. Copper S. W. Doroff, pp 371-88, Arlington, Va.: Office of Naval Reseaarch-Department of the Navy, 1974.

[37] Faltinsen, O. M., *Hydrodynamics of High-Speed Marine Vehicles*, Norwegian University of Science and Technology, Cambridge University Press, September 2009.

[38] Wagner, H., *Über Stoss- und Gleitvorgänge an der Oberfläche von Flüssigkeiten*, Zeitschr. f. Angew. Math und Mech, 12, 4, 193235, 1932.

[39] Kochin, N. E., Kibel, I. A., Roze, N. V., *Theoretical Hydromechanics*, New York: Interscience Publishers, 1964.

[40] Sclavounos, P. D., *Nonlinear impulse of ocean waves on floating bodies*, Department of Mechanical Engineering, Massachusetts Institute of Technology, Cambridge, MA 02139, USA, 2012.

[41] Newman, J. N., *Marine Hydrodynamics*, The MIT Press Cambridge, Massachusetts, and London, England, 1977.

[42] Endresen, P.C., *Vertical Wave Loads and Response of a Floating Fish Farm with Circular Collar*, Norwegian University of Science and Technology, June 2011.

[43] Greco, M., *TMR 4215: Sea Loads, Lecture Notes*, DEPT. OF MARINE HYDRO-DYNAMICS, NTNU, 2012.

[44] Riste, K. B., *Development of a Frequency-domain Model for Dynamic Analysis of the Floating Wind Turbine Concept-WindFloat*, Norwegian University of Science and Technology, June 2016.
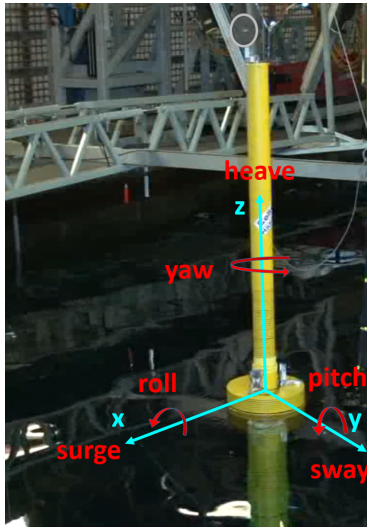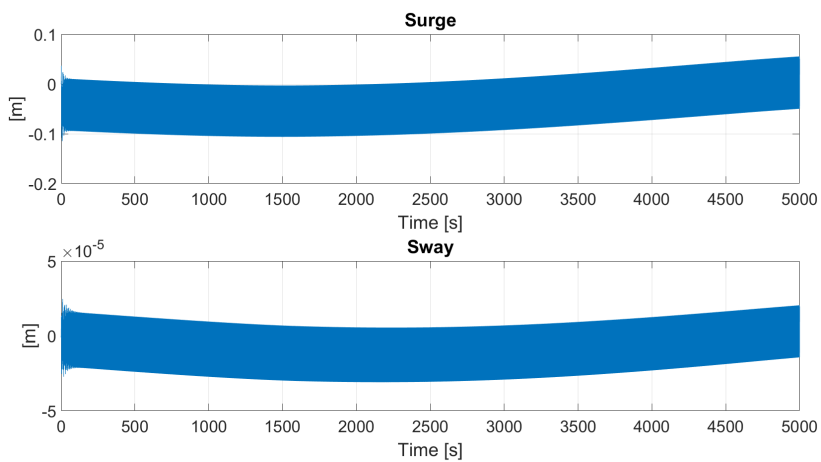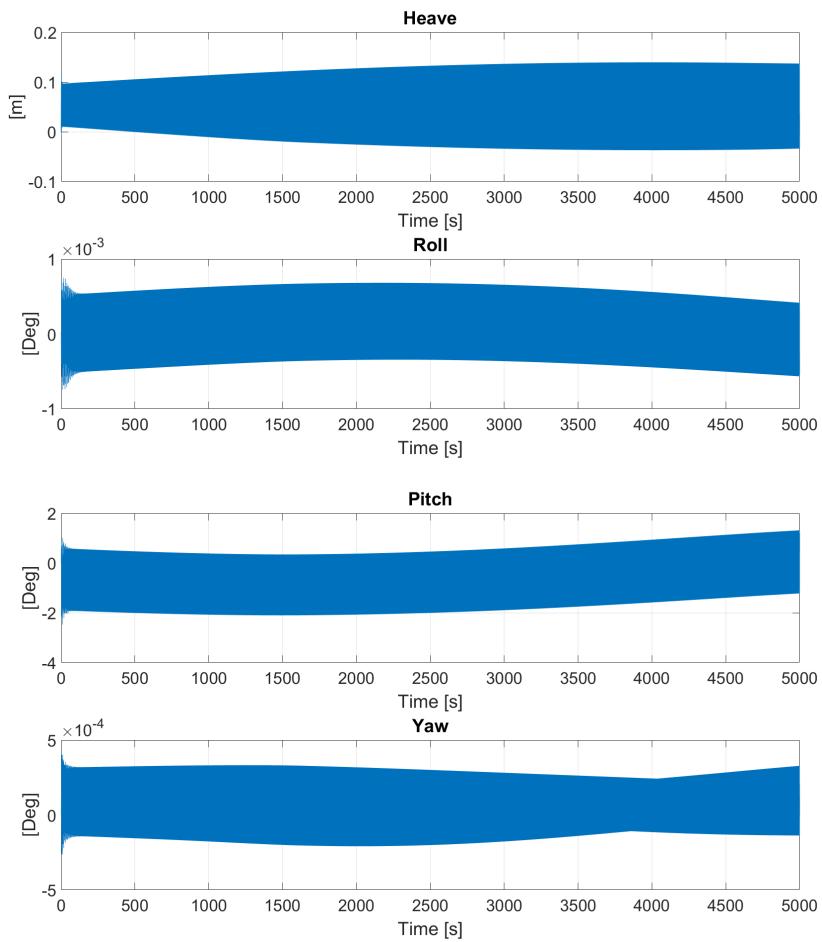
Appendix

Global total position of the STC

Figure 6.1: STC coordinate system with the definition of motions in the 6 D.O.F..

6.3.1 Case with H=9 m and T=11 s

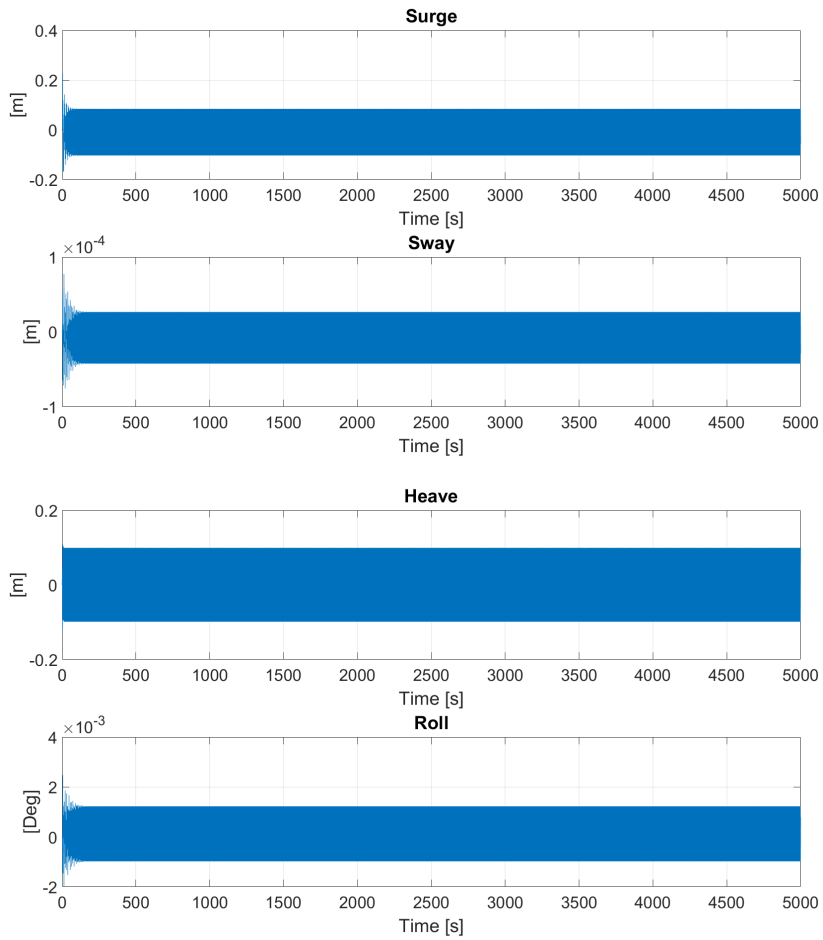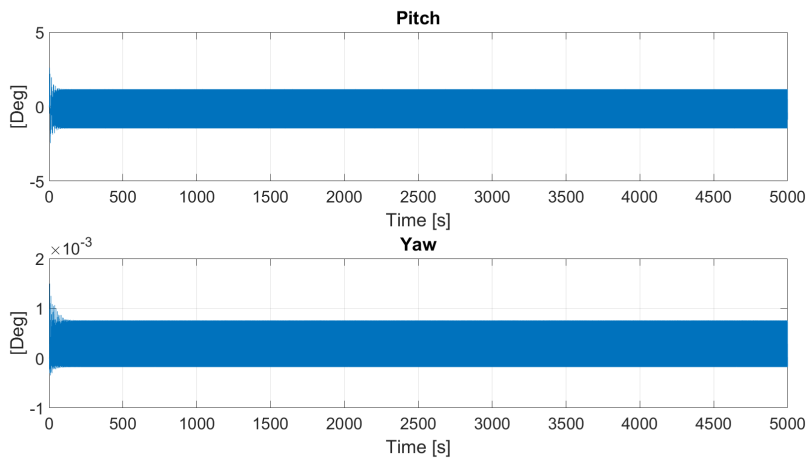**Figure 6.2:** 6 D.O.F. motions for the case with H=9 m and T=11 s.

6.3.2 Case with H=9 m and T=23 s

Figure 6.3: 6 D.O.F. motions for the case with H=9 m and T=23 s.